Luminance and Contrast adaptation of the Inner Retina

Inauguraldissertation

zur

Erlangung der Würde eines Doktors der Philosophie

vorgelegt der

Philosophisch-Naturwissenschaftlichen Fakultät

der Universität Basel

von

Miguel Henriques dos Santos Caracol Teixeira

aus Portugal

Basel, 2015

Original document stored on the publication server of the University of Basel

edoc.unibas.ch

Genehmigt von der Philosophisch-Naturwissenschaftlichen Fakultät

auf Antrag von

Prof. Dr. Silvia Arber

Dr. Botond Roska

Prof. Dr. Karl-Klaus Conzelmann

Basel, den 25 März 2014

<div style="margin-left:50%">

Prof. Dr. Jörg Schibler

Dekan

</div>

Table of Contents

Abstract

Adaptation is a common feature of sensory systems, matching neural activity to the range of inputs from the environment. In the visual system this is of great importance because visual stimulus can change across 9 orders of magnitude. In this context the visual system attempts to match both the magnitude and variance of the input to the range of neural activity of its component neurons. This adaptation to the environment begins during the first stage of visual computations of vision, in the retina. In this thesis I have focused on how circuit mechanisms of adaptive processes are computed in the retina. There are ~20 different circuits and each circuit extracts an individual feature of the visual stream. Specific mechanisms of adaptation were isolated in some of these neuronal circuits. First I studied how ganglion cells adapt to different light intensities, and identified a circuit responsible for a switch-like component between two distinct states that implements distinct perceptual regimes at different light levels. In the second part I investigated how identified neuronal circuits respond to contrast adaptation, showing that different ganglion cells respond differently to changes in contrast. I was able to show that identified ON cell types adapt to changes in contrast, while and OFF cells do not. In the third part of my thesis I was involved in the development of a tool that allows cell type specific manipulation of circuits called Transcription Devices Dependent on GFP (T-DDOG) based on camelid antibodies. I demonstrated its relevance by using it to express optogenetic tools to drive a light response in a specific cell class of the retina, bipolar cells.

Introduction

The mammalian retina has many output channels connected to higher brain regions called ganglion cells. These ganglion cells are historically difficult to differentiate so adaptive processes were often generalized and lumped together. With the use of new genetic technologies, molecular biology and virology tools, we were able to perform targeted recordings of individual cell types and dissect the elements of the circuit involved in forming each output. Here I investigate the adaptive processes involved in the adaptation to magnitude of light and isolated a phenomenon involving a special neuronal circuit present in the retina. I also studied the adaptation to contrast change where cell type differentiation was not found but we found an interesting difference between two subclasses of ganglion cells. In addition, I contributed to the foundation of a novel technology that allows a protein normally used for tagging cells, GFP to manipulate genes.   In this thesis I developed and made use of new techniques that are able to isolate single circuits in the retina, improving our grasp as to how the retina discriminates different features of the visual field and how it adapts to changes in these features.

The mammalian retina

The mammalian retina is composed of a stratified layer structure where 5 different classes of retinal neurons are interconnected, combining to extract the visual world into specific features that are then transmitted to the higher brain regions(Masland 2001a)(Masland 2001b).

Photoreceptors are located in the outer nuclear layer, furthest from the stimulus, making the light travel through the retina to be captured. Two different types of photoreceptors are present in this layer, rods and cones. These cells types are responsible for transforming photons to electrical signals. Cones are specialized in capturing photons in daylight, or photopic conditions, and capture photons at different spectral sensitivities, enabling the visual system to perceive color. Rods normally operate in dim light, or

scotopic conditions, and only capture light in one spectral condition. In mesopic conditions both photoreceptors are active. Photoreceptors always release glutamate in the dark, and respond to increments of light with hyperpolarization of the membrane potential that reduces the rate of glutamate release. They transmit these signals to a class of cells called bipolar cells at synapses located within the outer plexiform layer of the retina.

In the inner nuclear layer approximately ten types of bipolar cells(Ghosh et al. 2004)(MacNeil et al. 2004) are present and these are divided into three different categories. ON bipolar cells that respond to increases of light. OFF bipolar cells, that respond to decreases of light(Bloomfield & Miller 1986). Rod Bipolar cells that are uniquely connected to Rod photoreceptors (Dacheux & Raviola 1986)(Bloomfield & Dacheux 2001). Bipolar cells carry information from the outer plexiform layer to the inner plexiform layer, where ganglion cell types then transmit this information to higher brain regions.

Ganglion cells are located in the ganglion cell layer and their dendrites stratify in the inner plexiform layer where they receive input from bipolar cells. Each ganglion cell type stratifies their dendrites in thin layers of the inner plexiform layer and only receives input from a specific selection of bipolar cells that co-stratify in the same layer. Since they are separated by stratification it is easy to identify, with the ON bipolar cells terminating closer to the ganglion cell layer and the OFF bipolar cells terminating closer to the inner nuclear layer. Ganglion cells have different dendritic trees morphologies and in combination with dendritic stratification we can distinguish cell types enabling us to record from specific cells types and extract the specific cell types features transmitted to the rest of the brain by the means of action potentials(Kong et al. 2005).

Two classes of inhibitory neurons also make up the retina, one present in the synapse between the photoreceptors and bipolar cells in the outer plexiform layer called horizontal cell and another called amacrine cell located in the inner plexiform layer. Horizontal cells extend laterally across the retina, and their axons connect specifically to rods and their dendrites to cones. Horizontal cells are depolarized by the release of glutamate from photoreceptors, giving inhibitory feedback to photoreceptors. There are

roughly 30 different cell types of amacrine cells(Masland 2001b), mostly inhibitory, it is the most diverse cell class in the retina, this group is divided into narrow field amacrine cells, medium and wide-field accordingly to their morphology, normally the narrow-field amacrine cells are glycinergic(Wässle et al. 2009) and the medium and large field amacrine cells are mostly GABAergic, interestingly some wide-field amacrine cells are spiking cells(Lin & Masland 2006).

In scotopic and mesopic conditions, where there is rod mediated light responses, the transmission pathway is changed since the rod bipolar cells do not connect to retinal ganglion cells. A specialized narrow-field amacrine cell is responsible for the transmission of information from rod bipolar cells to the rest of the other cones bipolar cells, this amacrine cell is called AII(Protti et al. 2005)(Bloomfield & Völgyi 2004). This type of amacrine cell makes an electrical synapse with ON bipolar cells and a glycinergic synapse to the OFF cone bipolar cell(Wässle et al. 2009). This detour through AII-cone bipolar cell loop allows the rod pathway to take advantage of the cone bipolar circuitry in the IPL, allowing the more sensitive rod pathway to transmit similar information as the cone pathway(Bloomfield & Dacheux 2001).
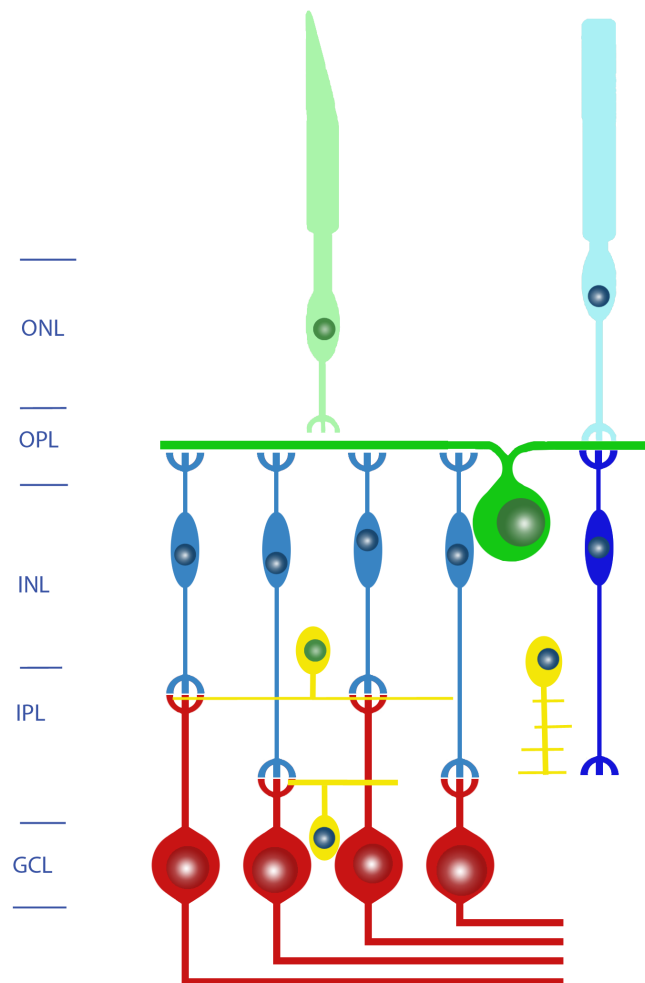
Schematic of the retina. ONL, outer nuclear layer; OPL, outer plexiform layer; INL, inner nuclear layer; IPL, inner plexiform layer; GCL, ganglion cell layer.

Light adaptation and ganglion cell types

The visual environment around us consists of different features including overall luminance, color, movement and contrast. These features are extracted and encoded by the retina. They vary in time and space and often these variations exceed the dynamic range of the neural network in the retina. One example is the overall light intensity that reaches the retina: it can vary from individual photons (star gazing) to a rain of photons on a sunny day, covering approximately nine orders of magnitude. Normally the retina computes visual information across different light conditions, in other words it can adjust the range in which it can operate from a dark room into the sunlight on a beach and vice-versa. How does the retina achieve this? It could adjust the working mode such that the neural signal evoked by any given feature

falls into the dynamic range of the system. That means either increasing sensitivity, when returning from bright sunlight into a dark room, or avoiding saturation when moving from a dark to bright environment. We call these processes adaptation. Adaptation is the act of modifying the response to a constant feature of the stimulus over time. The above-mentioned adjustment, adaptation, does by no means exist only in the visual system. Many other sensory systems perform the same adjustment to the stimulus (Kurahashi & Menini 1997; Lanting et al. 2013).

Adaptive processes in vision can be found on different levels and multiple places. Some of these processes simply regulate the number of photons hitting the retina, processes like contraction and dilation of the pupil(Pennesi et al. 1998) achieve this purpose. Others adaptive processes adjust the sensitivity at the level of photoreceptors or downstream neural circuitry, either in the retina or visual cortex. Processes like the amplifications of the phototransduction cascade(Pugh & Lamb 1993), diminished ganglion cell receptive fields surrounds(Barlow & Levick 1969), decrease in ganglion cell's firing rate responding to a constant stimulus(Enroth-cugell & Lennie 1975b) and changes in cortical processing(Yang & Stevenson 1999). All these processes improve the visual system performance at new light conditions.

Contrast adaptation

The visual system also has to take into account big fluctuations relative to the mean, or contrast. Depending on the amount of contrast present the ganglion cells response changes. When the contrast in the environment is very weak, adaptation increases sensitivity to improve signal-to-noise ratio. When the contrast is very strong the ganglion cells response decreases in order to prevent saturation and loss of information.

Two types of contrast adaptation are known to happen in the retina, fast and slow contrast adaptation. Fast contrast adaptation, also called "contrast gain control" affects the moment-to-moment response in the retina(Victor Jonathan D. 1987). For example it can prevent the saturation of retinal output as the eye scans over reflection highlights or dark shadows in

the visual scene. Fast adaptation also has a profound effect on how the retina processes moving stimuli(Berry II et al. 1999). Slow contrast adaptation occurs over many seconds, during which time there are many eye and head movements occur. This prolonged modulation adjusts retinal sensitivity to the overall contrast level existing in the visual scene. Such slow adaptations are already described in the literature mainly by psychophysics experiments(Blakemore et al. 1969). Our retina is thought to be a major player in slow contrast adaptation(Chander & Chichilnisky 2001) (Truchard et al. 2000) (Demb 2008).

Chapter 1. Ambient illumination toggles a neuronal circuit switch in the retina and visual perception at cone threshold

Introduction

The mammalian visual system operates over a large range of light intensities that challenge it with input regimes in which either individual photons must be gathered to reconstruct the visual scene or salient features need to be extracted from the flux of billions of photons(Hood & Finkelstein 1986; Rieke & Rudd 2009). At low light intensities, it collects photons using only the highly sensitive rod photoreceptors, at medium intensities, rod and cone photoreceptors are both at work, while at high intensities, only cones are used. In these three regimes, the visual system gathers information using ≈20 discrete visual channels that originate with mosaics of local neuronal circuits in the retina(Masland 2001b; Wässle 2004). The neurons that carry the output of these circuits are the ≈20 distinct ganglion cell types, each of which highlights a unique feature of the visual scene(Berson 2008; DM 1994; Farrow & Masland 2011; Levick 1967; Roska & Werblin 2001). During the transition from starlight to bright daylight conditions, a number of adaptive processes increase the acuity and contrast sensitivity, as well as affect the spatial integration properties of the visual system. These changes have been observed in the retina(Barlow et al. 1957; Bisti et al. 1977; Enroth-cugell & Robson 1966; Muller JF 1997; Peichl & Wässle 1983; Rodieck & Stone 1965) lateral geniculate nucleus(Bisti et al. 1977; Ramoa et al. 1985; Virsu et al. 1977; Wiesel & Hubel 1966), and visual cortex(Bisti et al. 1977; Ramoa et al. 1985), as well as during visual perception(De Valois et al. 1974; Kelly 1972; Pasternak & Merigann 1981; Umino et al. 2008; Van Nes et al. 1967).

In the retina, the receptive fields of most ganglion cells are organized into center and surround regions, where illumination of the surround reduces the sensitivity of the ganglion cell to center illumination(Barlow 1953)(Kuffler 1953). Soon after center-surround receptive fields were first described in the retina(Barlow 1953; Kuffler 1953), it was noted that in dark adapted states the antagonistic surround of some ganglion cells was weak or disappeared

completely(Barlow et al. 1957; Bisti et al. 1977; Dedek et al. 2008; Enroth-cugell & Robson 1966; Muller JF 1997; Rodieck & Stone 1965). However, other studies have reported that the antagonistic surround is maintained in dark-adapted states(Enroth-cugell & Lennie 1975a; Troy et al. 1999). These discrepancies have not been resolved, since, with the exception of recordings from X ganglion cells in the cat(Bisti et al. 1977; Enroth-cugell & Lennie 1975a; Enroth-cugell & Robson 1966; Troy et al. 1999), experiments could not reproducibly target an individual ganglion cell type. The neuronal circuitry forming the ganglion cell's antagonistic surround involves lateral inhibitory signaling pathways that allow adjacent columnar circuits in the retina to interact(Wässle 2004). These pathways are mediated by horizontal cells in the outer retina and amacrine cells in the inner retina(Cook & McReynolds 1998; Flores-Herr et al. 2001; Ichinose & Lukasiewicz 2005; Mangel 1991; McMahon et al. 2004; Naka & Witkovsky 1972; WR. 1999; Werblin 1974).

The circuit mechanism underlying the luminance-dependent strength of ganglion cell inhibitory surround, its specificity for certain types of ganglion cells, and whether these changes occur continuously or abruptly across luminance levels have remained in question. Here we show that the organization of the center and surround of specific types of ganglion cells exist in two discrete states. At low ambient light levels, these ganglion cells have a weak surround, and at higher levels, they have a strong surround. The switch between states is abrupt and reversible, occurring at light levels at which cone bipolar cells are strongly activated. The switch is implemented by the activation of large inhibitory spiking amacrine cells that provide input to ganglion cells. Consistent with the data, we present a model describing how the retina could combine electric transmission and spike threshold to switch inhibition on and off. Finally, we show that human spatial vision can also be reversibly toggled between two discrete states around cone threshold. We discuss the similarities between the luminance-dependent changes in spatial vision and the neuronal responses of the ganglion cells in the retina.

Results

A Switch-like Change in the Receptive Field Structure of a Retinal Ganglion Cell

We performed two-photon laser targeted patch clamp recordings from labeled ganglion cells in isolated retinas of transgenic mice where eight types of ganglion cells express a fluorescent protein (Experimental Procedures, Figure S1-S3)(Feng et al. 2000; Hippenmeyer et al. 2005; Madisen et al. 2010; Münch et al. 2009). Across eight logarithmic units of light intensity we presented spots of different sizes to the retina with the same positive contrast, but at different background light levels, while recording either the spiking responses in loose cell attached mode, or voltage responses in current clamp mode. One cell type, the PV1 cell, responded to small spots of positive contrast with sustained spiking or depolarizing voltages (Figure 1.1A), a response consistent with its dendritic arborization in the proximal part of the inner plexiform layer (Figure S1).
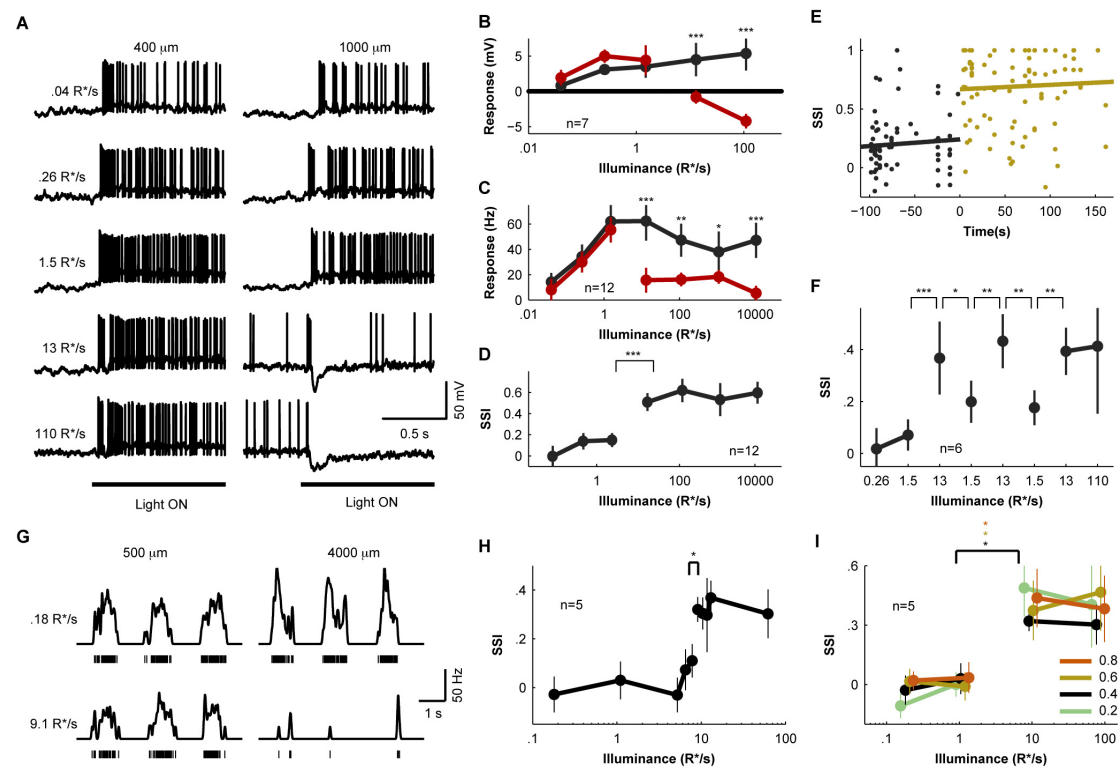
Figure 1.1. Switch-like change in the receptive field organization of PV1 cells.
A. Current clamp recordings of membrane voltage from a PV1 cell. Responses to the

presentation of 400 μm (left column) and 1000 μm (right column) spots across five log units of light intensity. The Michelson contrast at each light level was 0.9993. Black line: time when the spots are presented. Light levels of the stimulus are shown, and are expressed as photons absorbed per rod per second (R/s). **B.** Summary of voltage recordings. Response of PV1 cells is taken as mean membrane potential +/- s.e.m. during first 1.5 seconds of spot presentation. **C.** Summary of spike recordings in loose cell configuration. Response is mean firing rate +/- s.e.m. during the first 1.5 seconds of the spot presentation. In **B** and **C**, data from the presentation of 400 μm (black) and 1000 μm (red) spots are shown. Throughout all figures, a break in the curve represents a statistically significant, P < 0.05, difference from the response at the previous light level. **D.** The spiking responses of PV1 cells to the small and large spots was compared using a spatial selectivity index (SSI, defined in Experimental Procedures) across the different background light levels. The SSI is low when the spiking response to small and large spots is similar and high when the spiking response to small spots is larger than the response to large spots. From the data plotted in **A - D,** we determined that there was a critical light level between 1.5 and 13 R*/s where the selectivity of the PV1 cell for small spots is switched on. **E.** Black points: SSI during single recordings at 1.5 R*/s at various times before the light level was increased to 13 R*/s. Yellow points: SSI from single recordings presented at various times after the light level was raised to 13 R*/s. The correlation coefficients of the black and yellow data points are 0.07 and 0.05, respectively. This indicates that there is little or no adaptation of the selectivity of the PV1 cell after the light level was changed. The SSI increased from 0.20 +/- 0.03 to 0.69 +/- 0.03, P < 0.001. **F.** The SSI is determined as the light level was repeatedly shifted above and below the critical light level. The SSI of PV1 cells could be toggled between switch-OFF and switch-ON states repeatedly. Each point is the mean +/- s.e.m. **G.** Spike frequency (continuous traces) and spike responses (vertical lines) of a PV1 cell to a drifting grating with a temporal frequency of 0.5 Hz, Michelson contrast of 0.4 and a spatial wavelength of either 500 mm (left) or 4000 mm (right). **H.** The SSI is calculated from drifting grating experiments across background light levels, the contrast was kept constant at Michelson contrast of 0.4. The fine step sizes around the selectivity threshold shows the sharp luminance dependent switch in the receptive field organization of the PV1 cell. **I.** SSI calculated from drifting grating experiments at different contrast values: the switch is contrast independent. Different colors indicate different Michelson contrast values.*

When presenting a spot, the same size as the dendritic field of the PV1 cell, the response increased steadily with increasing background intensity (Figure 1.1A-C, S4). We found a remarkably different pattern of responses when presenting spots ~2.5 times the size of the dendritic field. Here, the voltage and spiking responses increased with increasing background intensity up to a critical light level (Figure 1.1A-C). However, at the next higher level, after a few spikes at stimulus onset, the membrane voltage changed polarity and the spiking output of the cell was reduced in a step-like fashion (Figure 1.1A-C). The hyperpolarizing voltage and reduced spiking responses remained stable at all brighter light levels. To quantify this luminance dependent change in PV1 spiking responses, we compared the spiking responses of PV1 cells to the small and large spots using a spatial selectivity index (SSI, defined in Experimental Procedures) across the different background light levels. The SSI is low when the spiking responses to small and large spots are similar and high when the spiking response to small spots is larger than to large spots. We found the SSI of the PV1 cell fell into one of two regimes: in low light conditions the PV1 cell had a low SSI; and at higher light levels the PV1 cell had a high SSI (Figure 1.1D). The background spiking of the PV cell had a mean of 5.9 Hz and was variable, likely depending on the light adaptation and stimulus history of the recorded cell, however the variation of background spiking between repetitions recorded from the same cell was low (Figure S4).

The transition from low to high spatial selectivity was abrupt, occurring with full effectiveness in less than 10 seconds, the minimum time we could probe the cells between the two conditions (Figure 1.1E). In addition, the transition was reversible: the spiking response could be toggled between two distinct states by shifting the background light levels up and down one log unit (Figure 1.1F). The change in spatial selectivity is independent of stimulus and contrast, since we observed a similar change for drifting gratings of different spatial frequencies at different contrasts (Figure 1.1G-I, S4). Fine resolution stepping through background intensities revealed that the significant change occurs across a change of intensities of 0.07 log units (Figure 1.1H). Quantifying spiking responses to spatio-temporal white noise stimuli also

revealed differences in linear receptive field structure at low and high intensities (Figure S4). Therefore, the spatial integration properties of the PV1 cell shifted abruptly and reversibly at a specific "critical" light level like a switch. We refer to the state of the circuit as "switch-ON", when the SSI is high and "switch-OFF" when it is low.

We found that a switch-like change in responses across light levels is not a universal property of retinal ganglion cells. While among PV cells (Figure 1.2 and S1) two large ganglion cell types, PV1 and PV6, showed an abrupt change in their spatial selectivity around the same background light level (Figure 1.3A and B), other ganglion cell types, most of them with smaller dendritic fields, had either no change in their responses or the responses were continuously changing with increasing background light level (Figure 1.3C and D).

A. Visual responses of PV cells
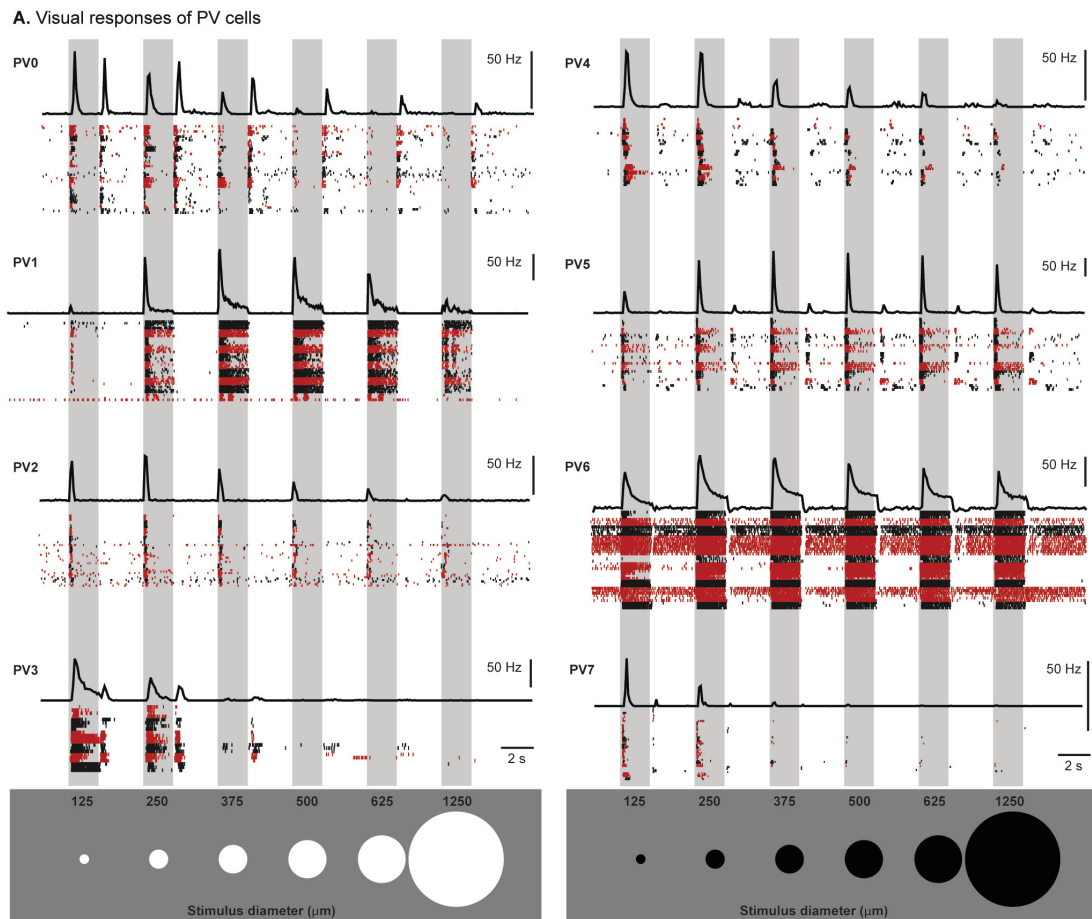
Figure 1.2. Visual response properties of PV cells.

A. The stimulus was a spot presented for two seconds with sizes of 125, 250, 375, 500, 625 and 1250 mm. The gray bars show stimulus timing. For each cell type the mean firing rate (50 ms bins) is shown above the raster plots from individual cells. Different cells are shown in alternating red and black colors. Within each color group each row is an individual recording. We repeated recordings from each cell 3-6 times. Altogether, recordings from 83 PV cells are shown. The stimulus for the four cells on the left was an increase in luminance, while for the four cells on the right the stimulus was a decrease in luminance, each on a gray background. The intensity of the gray background was 5000 R*/s and the Michelson contrast were 0.3. We relate the eight PV cell types to mouse ganglion cell types reported in the literature. Note that in some cases the relationship is speculative and, therefore, for each relationship we add a subjective number between 0 (speculative) and 1 (confident) that quantifies the likeliness of correspondence. PV0: ON-OFF directional selective ganglion cell, symmetric type (0.99)(Huberman et al. 2009; Kay et al. 2011), PV1: ON-Alpha cell (0.8)(Pang et al. 2003) or M4 (0.8)(Ecker et al. 2010; Estevez et al. 2012), PV2: ?,

18

PV3: W3 cell (0.8)(Zhang et al. 2012)*, PV4:?, PV5: OFF Alpha transient cell (0.6)*(Huberman et al. 2008; Münch et al. 2009; Pang et al. 2003)*, PV6: OFF Alpha sustained cell (0.8)*(Pang et al. 2003)*, PV7: JAMB cell (0.99)*(Kim et al. 2008)*.*
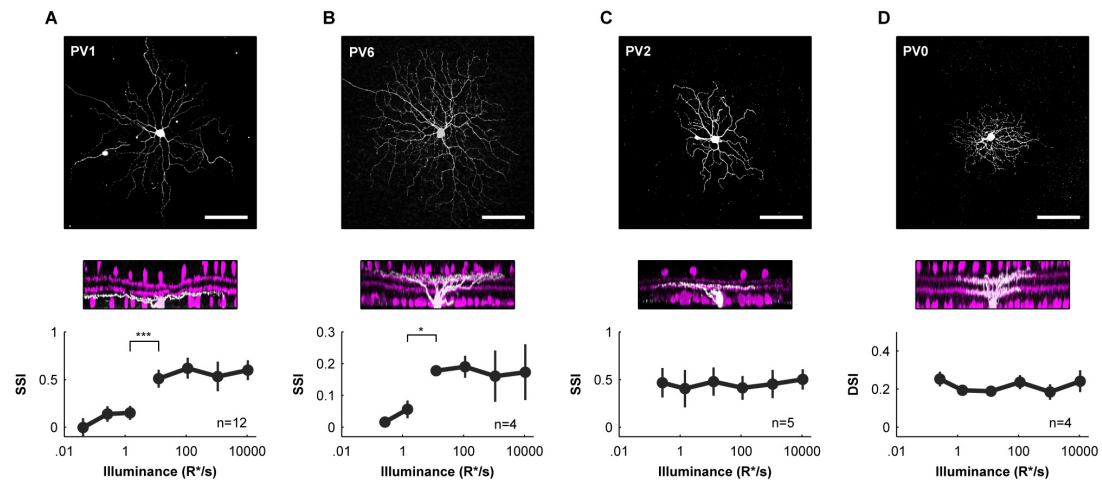
Figure 1.3. The morphology and spatial selectivity of selected PV cells.

The morphology of PV1 (A), PV6 (B), PV2 (C) and PV0 (D) retinal ganglion cells are summarized. Top panels: top view of example PV cells. The scale bar represents 100 μm. Middle panels: z-projection (white) overlaid on an antibody staining of ChAT-expressing cells (magenta), which form two bands in the inner plexiform layer. Bottom panels: the spatial or direction selectivity of the ganglion cell across a range of light intensities. For PV1, PV6 and PV2 cells, the SSI, for PV0 cells the direction selective index (DSI) is shown. The PV1 and PV6 cells show a significant increase of the SSI as the light level is increased from 1.5 to 13 R*/s.

A Large Spiking Inhibitory Neuron is Activated by the Switch

How does such a strong change in circuit filtering occur at a specific light level? To determine the neuronal and synaptic elements involved we dissected the circuitry mediating this switch. As a first step, we asked whether inhibitory neuronal elements were required to actively suppress the response of the PV1 cell to the presentation of large spots at the critical light level and above, a likely scenario given the hyperpolarizing responses to the presentation of large spots at these light levels (Figure 1.1A and B). We found that the application of the GABA antagonist picrotoxin blocked the switch: in the presence of picrotoxin the responses to large spots were similar to the responses to small spots at the brighter light levels (Figure 1.4A and B).

19
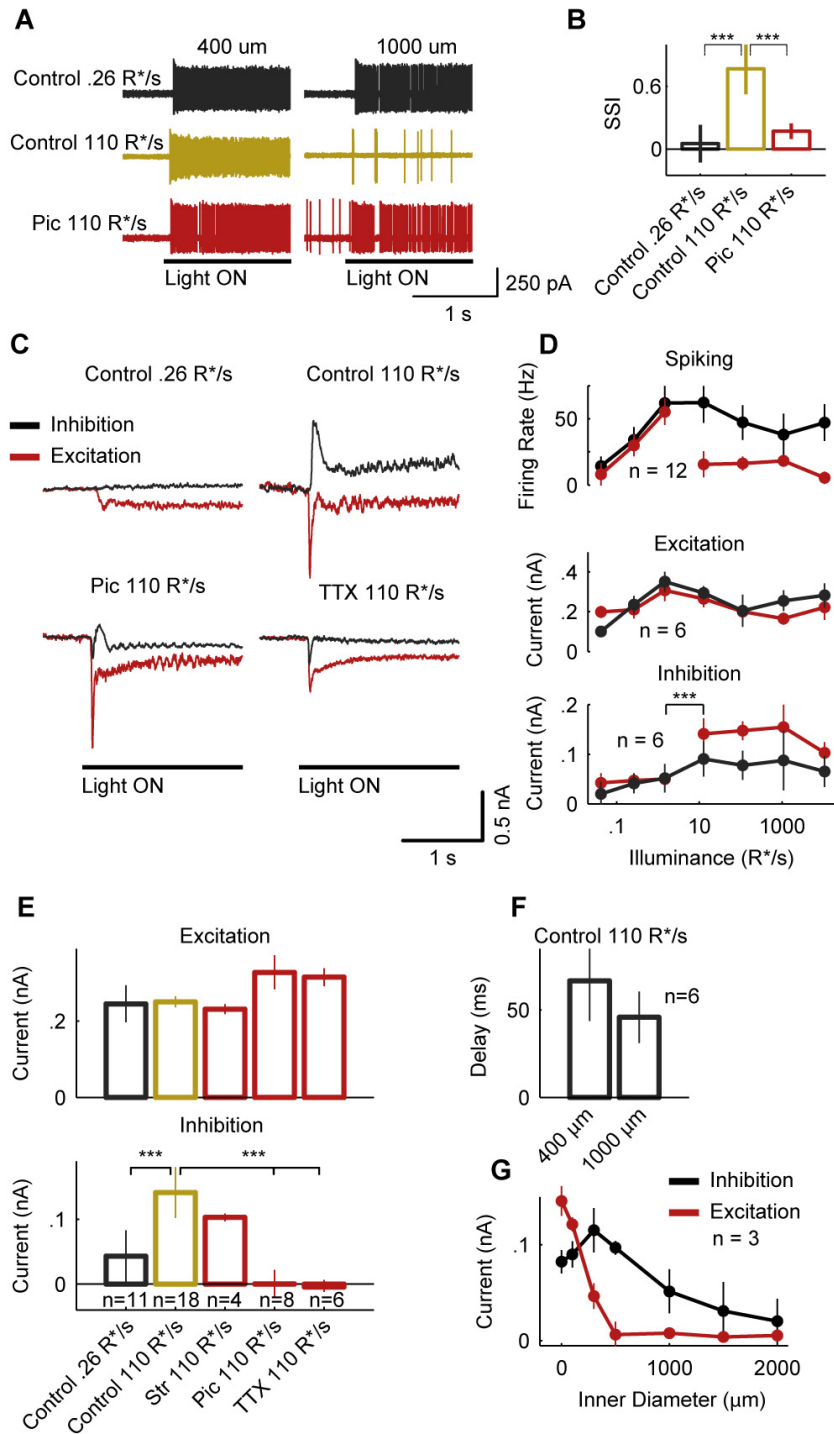
Figure 1.4. Switch-like change in the receptive field organization of PV1 cells is mediated by inhibition.

In **A** and **B** black indicates control experiments carried out under low-light condition of 0.26 R*/s, yellow are control experiments carried out in brighter conditions of 110 R*/s, and red indicates experiments carried out with a picrotoxin (Pic) at 110 R*/s. **A.** The spiking response of a PV1 cell to the presentation of either a 400 µm (left) or

1000 µm (right) spot. This was done in three conditions: low light (0.26 R/s), bright light (110 R*/s), and bright light (110 R*/s) with picrotoxin. The black line indicates when the spots were presented. **B.** Summary of spiking response of PV1 cells under the three conditions used in A. The SSI is shown (mean +/- s.e.m.) for the three conditions. **C.** Excitatory and inhibitory input currents (Experimental Procedures) to the PV1 cell in control conditions, in TTX and in picrotoxin (Pic). The black bar indicates when the 1000 µm spot was presented. Each trace is the average of three recordings. **D.** Summary of input currents recorded during the presentation of a 400 µm (black) or 1000 µm (red) spot across ambient light intensities. Data are presented as the mean +/- s.e.m. Top panel: spiking response replotted from Figure 1C. Middle panel: excitation. Bottom panel: inhibition. **E.** Summary of input currents recorded during the presentation of a 1000 µm spot in different conditions. Data are presented as the mean +/- s.e.m. Top panel: excitation. Bottom panel: inhibition. **F.** Latency between peak of excitatory input and peak of inhibitory input. **G.** Excitatory (red) and inhibitory (black) input to PV1 cell responding to annuli with an outer diameter of 2400 µm and inner diameter ranging from 0 to 2000 µm (x axis). In this and other figures, inhibition and excitation refers to currents measured at 0mV and -60 mV, respectively, and these currents, unless indicated, were quantified taking the absolute value of the mean current during the first 0.5 s after stimulus onset (Experimental Procedures).*

Dopamine agonists and antagonists did not influence the switch (data not shown). Therefore, the switch involves the activation of inhibitory elements at a critical light level.

To ascertain if the inhibitory elements are acting directly on the ganglion cell we performed a set of voltage clamp and pharmacological experiments (Experimental Procedures, Figure S5). We recorded the input currents to PV1 cells at different holding potentials, and determined the stimulus-evoked excitatory and inhibitory inputs at switch-ON and switch-OFF circuit states. Our analysis revealed that an inhibitory conductance in the ganglion cell was strongly activated when the switch was toggled ON (Figure 1.4C and D). This inhibitory conductance was blocked with picrotoxin, a GABA antagonist, and TTX, which blocks sodium spikes in the retina, but not by strychnine, a glycine antagonist (Figure 1.4C and E). Inhibition was delayed compared to excitation (Figure 1.4F) and annuli up to 2 mm in

diameter were able to activate the inhibitory input at light levels at which the circuit is in the switch-ON state (Figure 1.4G). The excitatory input to PV1 cells did not show a discontinuous decrease in strength (Figure 1.4D), suggesting that horizontal cells are not responsible for the switch. Since amacrine cells mediate inhibitory input to ganglion cells, we conclude that the switch involves the activation of GABAergic spiking amacrine cells that can act from a distance and are directly connected to PV1 cells.

To confirm that far reaching amacrine cells directly connect to PV1 cells, we carried out monosynaptically restricted viral tracing using G-deleted rabies virus where the G protein is supplied to the PV ganglion cells by a conditional adeno-associated(Marshel et al. 2010; Stepien et al. 2010; Wickersham et al. 2010) or Herpes virus(Yonehara et al. 2011) (Figure S6). We reconstructed the transsynaptically labeled amacrine cells around three PV1 cells, each in a different mouse (Experimental Procedures), and found amacrine cells with long processes, some reaching over one mm across the retina, connected to PV1 cells (Figure 1.5, S6 and S7). These "wide-field" amacrine cells, revealed by monosynaptic tracing, are likely the inhibitory cells that are activated by the switch. Note that PV cells other than PV1 also receive input from wide-field cells and, therefore, the PV1 connecting amacrine cells must have special properties that allow the implementation of the switch(Lin & Masland 2006).
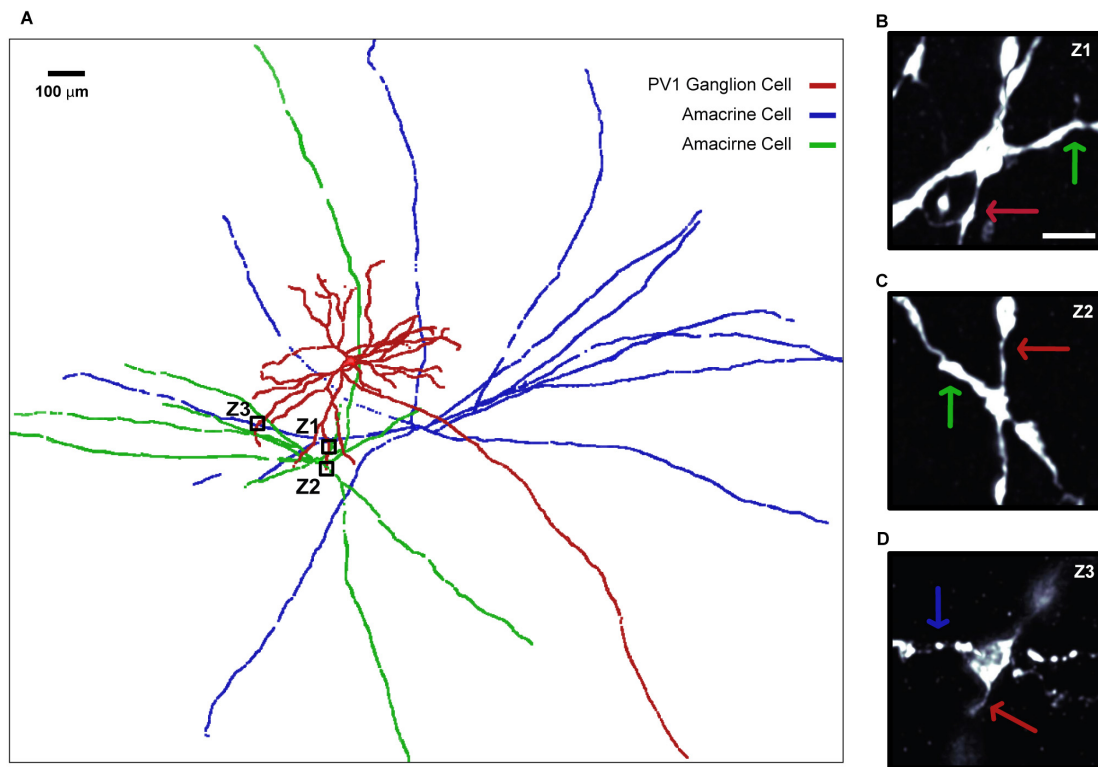
Figure 1.5. Monosynaptic retrograde tracing shows wide-field amacrine cells connected to PV1 ganglion cell.

A. *Examples of monosynaptically connected amacrine cells to a PV1 cell. Red: neurolucida tracing of rabies-labeled PV1 cell. Green and blue: neurolucida tracing of rabies-labeled amacrine cells (Experimental Procedures). The scale bar is 100 µm.*

B, C, D. *Zoomed-in images of the points of contact between the cells taken from the black boxes shown in A. The images are projected from a 1µm thick image stack. The scale bar is 2 mm.*

The Implementation of the Circuit Switch

How could inhibition be differentially activated in two different regimes of vision? The retina incorporates two kinds of photoreceptors, rods and cones, which provide the sensory interface for image-forming vision. The more sensitive rods and the less sensitive cones have overlapping light intensity ranges of signaling (Figure S2) and, therefore, three ranges can be defined: vision mediated by rods only, rods-and-cones and cones only. In order to determine whether the transition between switch-OFF and switch-ON states correspond to the transition from vision mediated by rods-only to rods-

and-cones, or rods-and-cones to cones-only, we recorded from rod and positive contrast activated cone bipolar cells in a retinal slice preparation (Figure 1.6A-C). We presented the slice with full-field steps of illumination with fixed contrast across different light intensities, incorporating rod-only and cone-only intensity ranges. The critical light intensity at which the switch was turned on corresponded to those light intensity values where cone bipolar cells became strongly activated. At this light intensity rod bipolar cells have already been fully activated. The critical light intensity was within the range reported to activate cones in mice(Nathan et al. 2006; Umino et al. 2008). These experiments are consistent with a view that the activation of cones toggles the switch (see Discussion for an alternative explanation).
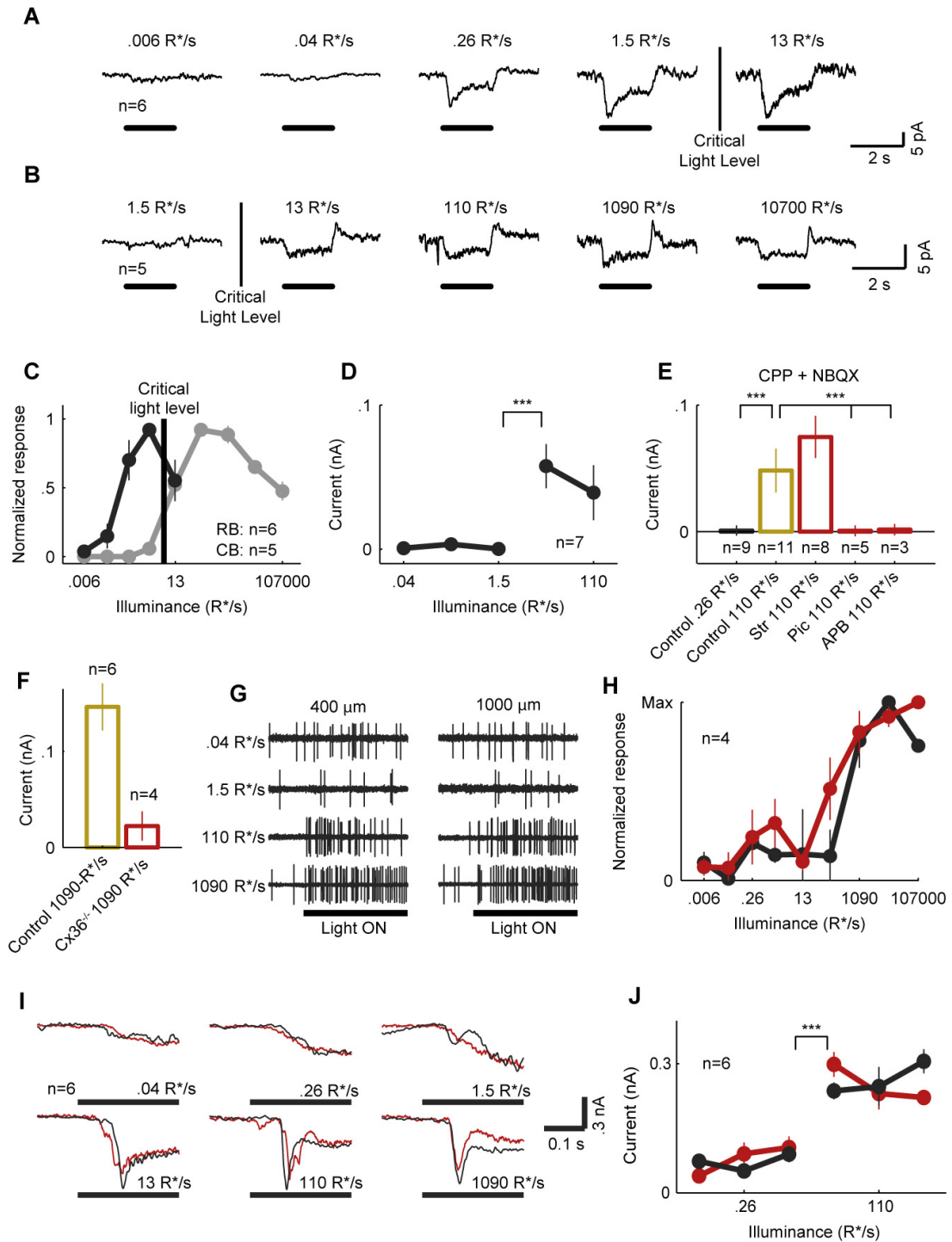
Figure 1.7. Amacrine cells are driven by cone bipolar cells via electrical coupling.

A-B. *Responses of bipolar cells, measured under voltage clamp at -60mV in slice preparation (**A**, cone bipolar cells, **B**, rod bipolar cells), to the presentation of full field stimuli across five log units of light intensity. The*

*Michelson contrast at each light level was 0.9993. Traces are averages across six (**A**) and five (**B**) recorded cells, respectively. **C.** Cone bipolar cells become highly*

*active at the critical light level that activates the switch. Black: rod bipolar (RB) cell responses grey: cone bipolar (CB) cell responses. **D.** Inhibitory input to PV1 cells in the presence of CPP and NBQX. At light levels below 13 R*/s no inhibitory current is seen in PV1 cells. At light levels of 13 R*/s and brighter a strong current appears. **E.** Pharmacology of inhibition in the presence of CPP and NBQX (referred to as "Control"). Stimulus is a 1000 μm spot. Black: inhibitory current recorded at 0.26 R*/s; yellow: current recorded at 110 R*/s; red: current recorded at 110 R*/s with, strychnine (Str), picrotoxin (Pic), or APB. **F.** Inhibitory input to PV1 cells in control (yellow) and Cx36^{-/-} (red) mice. **G.** Spiking response of PV1 cells to the presentation of small (400 μm) and large (1000 μm) spots in Cx36^{-/-} mice. **H.** Summary of spike recordings in Cx36^{-/-} mice. Spike frequency was normalized to the mean maximum response to different stimuli. Black: 400 μm spot; red: 1000 μm spot. Each point is mean +/- s.e.m. **I.** Excitatory currents to PV1 cells at different light levels after stimulus onset. Black: 400 μm spot; red: 1000 μm spot. Each trace is the mean response from 6 PV1 cells, each from a different animal. **J.** Mean excitatory current measured between 50 and 150 ms after stimulus onset from the traces in **I**. Each point is the mean +/- sem.*

Bipolar cells provide excitatory input to both ganglion cells and amacrine cells. How could bipolar cells continuously drive excitatory input to the ganglion cell, but independently instruct inhibition through wide-field amacrine cells in a discontinuous, switch-like way? To investigate whether the excitatory input to the PV1 ganglion cell and the inhibitory switch encompassing amacrine cells is mediated by the same or different mechanisms, we blocked glutamate signaling using CPP and NBQX, which are antagonists of the ionotropic glutamate receptors. As expected, the excitation to PV1 cells was blocked. However, at light levels when the switch is ON the inhibitory input remained, suggesting that the excitatory drive to the amacrine and ganglion cells is acting through a different mechanism (Figure 1.6D, E and S5). In the presence of NBQX and CPP, the inhibitory current was blocked by APB, which stops the response of those bipolar cells that respond to contrast increments (Figure 1.6E). As amacrine cells could be driven by electrical synapses rather than chemical synapses(Deans et al. 2002), we created a triple transgenic line in which both alleles of connexin36 were knocked out and the PV cells were labeled with EYFP. In this knock-out

animal we performed the same functional experiments as those that showed the switching filtering properties. Since connexin36 is needed for the rod signals to reach the amacrine and ganglion cells(Deans et al. 2002), there were no inhibitory or excitatory responses at low light levels, as expected. More importantly, the inhibitory input to PV1 cells decreased significantly (Figure 1.6F, S5) and the spiking responses of the PV1 cell to large and small spots remained similar across higher light intensities (Figure 1.6G and H). These results, taken together with the voltage clamp recordings (Figure 1.6D and E), suggest that the switching amacrine cells receive excitatory input via electrical synapses incorporating connexin36.

These experiments are consistent with cone bipolar cells providing input to switching amacrine and PV1 cells using different mechanisms but do not explain why the excitatory input to PV1 cells does not show a stepwise increase in strength at the critical light level (Figure 1.4D). In order understand this we examined the time course of the excitation to PV1 cells. The quantification of responses thus far incorporated a long time scale, using average responses across a 0.5 second time window. When we quantified excitation in a shorter time window after stimulus onset, the strength of excitation also showed a stepwise increase at the critical light level (Figure 1.6I and J) and a few spikes were detectable transiently after the onset of the light stimulus (Figure 1.1A and S4). These findings, together with the observed delay between inhibition and excitation (Figure 1.4F), are consistent with an excitatory input from cone bipolar cell terminals that also shows a stepwise increase at the critical light level, but is then silenced after a delay by the action of an inhibitory cell turned on at the same light level. Indeed, the application of picrotoxin and TTX both resulted in an increase of the average excitatory input to the PV1 cell (Figure 1.4E), suggesting that spiking, GABAergic amacrine cells mediate this inhibition to cone bipolar cells. Note, however, these increases did not reach the threshold for statistical significance. A possible circuit mechanism explaining the lack of significant increase is the mutually inhibitory interaction between GABAergic and glycinergic inhibitory cells (Roska et al. 1998; Zhang et al. 1997). The blockage of GABAergic inhibition mediated by large spiking GABAergic amacrine cells may have caused an increase of glycinergic inhibition from

small amacrine cells (Wässle et al. 2009) that acted on bipolar terminals to inhibit glutamate release. This increase in glycinergic inhibition may have compensated for the expected increase in excitatory input to ganglion cells.

From these experiments we put together the following model for the circuit switch of PV1 cells (Figure 1.7). PV1 cells receive inhibitory input from a set of wide-field, GABAergic spiking amacrine cells that we call switch cells. PV1 and switch cells receive excitatory input from cone bipolar cells, either the same or different types. Bipolar cells drive PV1 cells via chemical synapses and the switch cells using electrical synapses (some of their input may also come from chemical synapses). As light levels increase from starlight to daylight conditions, an object with the same contrast evokes increasing activity in cone bipolar cell terminals. The bipolar-to-PV1 cell gain is high (chemical synapse) but the bipolar-to-switch cell gain is low (electrical synapse) and, therefore, the excitatory drive reaches a threshold in PV1 cells, but not the switch cell. An additional factor contributing to the sensitivity of PV1 cells to detect small changes in cone bipolar cell activity is that the resting potential of PV cells is close to their spike threshold (data not shown). At a critical light level the input to cone bipolar cells suddenly increases, and the cone bipolar cell terminals experience a similar increase in their input. The sharp increase in drive to bipolar terminals leads to a similarly sharp increase in the excitatory drive to switch cells, lifting the voltage above the spiking threshold, resulting in inhibitory input to the PV1 cell. The relative contribution of inhibition and excitation is dependent on the size of the spot stimulus presented. The excitatory input saturates when the size of the spot is larger than the dendritic field of the PV1 cell, while the inhibitory input continues to increase with increasing spot diameter. This results in a smaller contribution of inhibition for small spots, but for large spots the contribution of inhibition is much larger, significantly decreasing the PV1 cell's response. As far as the dynamics of the switch-circuit, inhibition is delayed compared to excitation, because the switch cell needs time to reach spike threshold, while excitation from bipolar cells is modulated without a threshold. In a brief time window after stimulus onset, before the activation of the switch cell, excitation to PV1 cells shows a similar sharp increase in strength as the time-averaged

inhibition. However, the time-averaged excitation does not show a stepwise increase at the critical light level because the switch cells also act at bipolar terminals and dampen the rise in excitation. Note that a chemical synapse is a complex non-linear filter and therefore the shape and magnitude of excitation in PV1 cell is likely not the same as the excitation experienced by the switch cell. This is important because excitation to switch cells has to be larger in switch-ON states than in switch-OFF states even at longer time scales, otherwise the switch would turn off. A quantitative model describing the circuit illustrates how the stepwise increase in the strength of inhibition toggles the weighting of center and surround interactions of the PV1 cell (Figure 1.7C and D, Figure S8).
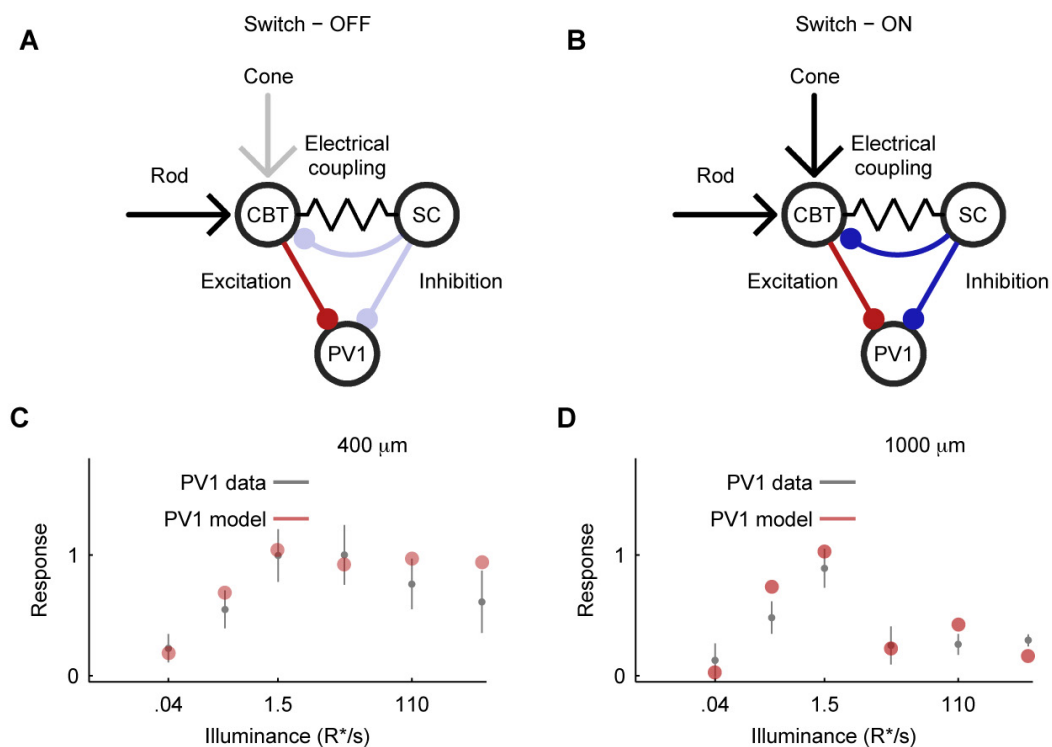
Figure 1.7. Key components of the switch (*a detailed model is shown in Figure S8).*

*In **A** and **B** light shading indicates inactive circuit connections, while dark shading indicates active connections. **A.** Schematic of connectivity of circuit during switch-OFF (low light) conditions. Cone bipolar cell terminals (CBT) are driven via rods. Note that rod signals can reach CBTs via rod bipolar cells (main route in mice) and via coupling to cones. CBTs provide excitatory drive to the PV1 ganglion cells via chemical synapses, and the switch cells (SC) via electrical synapses. Switch cells*

are only weakly excited and, do not reach spiking threshold. The inhibitory input to PV1 cells and to CBTs therefore remain inactive. **B.** *Schematic of connectivity of circuit during switch-ON conditions. CBTs are driven by rods and cones, or only cones. CBTs provide excitatory drive to PV1 cells via chemical synapses, and the switch cells via electrical synapses. Switch cells are excited more strongly, reaching spiking threshold and, therefore, activating inhibitory input to PV1 cells and CBTs.* **C, D.** *Quantitative models reproduce basic results of experiments (Experimental Procedures, Figure S8)*. *Grey: data from Figure 1C; red: model response.* **C.** *The model response and recorded data to the presentation of a 400 µm spot.* **D.** *The model response and recorded data to the presentation of a 1000 µm spot.*

A Perceptual Correlate of the Retinal Switch

Is there a perceptional correlate of the retinal switch, which toggles the balance of inhibition and excitation in large ganglion cell types of mice around the cone threshold? We investigated the transition of spatial integration properties of the human visual system across the rod only to rod-cone mediated vision ranges by measuring the contrast sensitivity for gratings of different spatial frequencies (called contrast sensitivity function, Figure 1.8A) together with the color discrimination abilities at different background light levels of 16 human volunteers. Color discrimination served as an internal control to detect cone photoreceptor activation. We quantified three aspects of visual perception from the measured set of contrast-sensitivity functions. Acuity was measured as the highest spatial frequency that could be detected at a given background light level; peak contrast sensitivity was defined as the maximum of the contrast-sensitivity function at a given light level, and a human spatial selectivity index (hSSI) was defined as the ratio between the contrast sensitivity at the lowest spatial frequency and the peak contrast sensitivity. We found that both the acuity and the peak contrast sensitivity increased continuously with increasing light levels (Figure 1.8B). However, the hSSI increased sharply as the background light intensity crossed a critical luminance threshold, dividing the curve into two regions (Figure 1.8C). This step-wise change corresponded to a sudden stop in the continuous increase in contrast sensitivity at low spatial frequencies (Figure 1.8A). The critical light level at which the hSSI increased in a step-wise manner corresponded

precisely to the light level where the volunteers could reliably discriminate between red and blue (Figure 1.8C). To test if the sudden jump in hSSI is reversible we measured the contrast sensitivity function as we increased and decreased the light level above and below the critical light level several times (Figure 1.8D). The hSSI reliably switched between the low and high values. Therefore, similar to switching on the inhibition in mice, a reversible step-wise change in hSSI corresponded to the light level where cones are activated, suggesting that the switch circuitry we describe in the mouse is likely conserved in human vision.
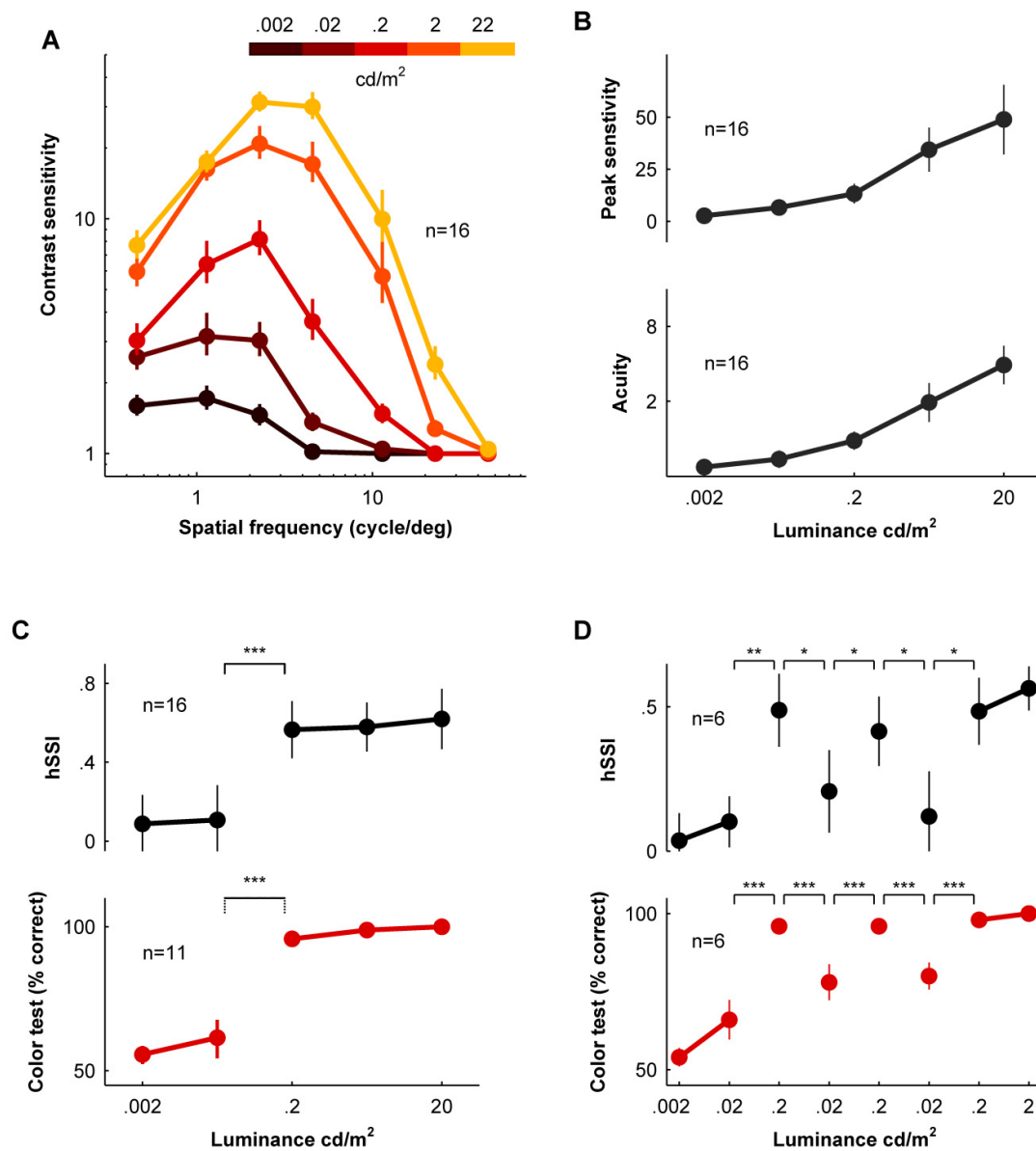
Figure 1.8. Switch-like change in human spatial vision.

A. Contrast sensitivity functions measured by threshold detection of sinusoidal

*gratings of different spatial frequency, at five different light levels from 0.002 cd/m^2 to 22 cd/m^2. Contrast sensitivity is defined as 1/threshold contrast. **B.** Continuously changing attributes of contrast sensitivity functions. Top panel: peak contrast sensitivity. Bottom panel: acuity. **C.** Discontinuous changing in spatial and color vision across light levels. Top panel: human spatial selectivity index (hSSI) switched states as the light level was increased from 0.02 to 0.2 cd/m^2. Bottom panel: threshold for reliable color discrimination corresponds with that of the change in the hSSI. **D.** Top panel: hSSI; bottom panel: ability of the volunteers to detect color. Both could be toggled between two states by shifting the light level from 0.02 to 0.2 cd/m^2.*

Discussion

A Neuronal Circuit Switch

By probing the receptive fields of identified retinal ganglion cells across light levels we found that PV1 and PV6 cell types, two large ganglion cells, show a step-like change in their spatial integration properties, consistent with the activation of an inhibitory surround. We concluded that the luminance dependent change in receptive fields of PV1 cells was caused by the activation of surround inhibition from wide-field spiking amacrine cells. The change showed characteristics of a switch: it occurred quickly, happened at a critical input level, and could be toggled between two distinct states. The critical light level that activated the switch corresponded to light levels where cone bipolar cells showed a stepwise increase in their responses.

Is the stepwise increase in cone bipolar cell responses a result of the activation of cones or, alternatively, an increase in the response of rods? In the first of these two situations, rod responses are saturated or close to saturation at the critical light level. Therefore it is the activation of cones that leads to the sudden change in cone bipolar activity. In the second, cones are not yet activated and it is an increase in rod activity acting via rod-cone electrical coupling(DeVries & Baylor 1995) that leads to the stepwise increase in cone bipolar cell responses.

We made four relevant observations to differentiate between these two scenarios. First, rod bipolar cells, which are driven by rods, are fully activated at light levels below the critical level (Figure 1.7A). Second, cone bipolar cells

are not responsive at light levels below the critical light level including those levels at which rod bipolar cells have reached saturation (Figure 1.7B). Third, the sustained part of the rod bipolar response, which could not have reached saturation since there were larger responses recorded, decreases at the critical light level (Figure 1.7C). Fourth, there is only one major increase in the responses of cone bipolar cells across the broad range of intensities tested (Figure 1.7B).

The activation of cones at the critical light intensity is consistent with these four observations. This interpretation is further supported by the fact that the critical light intensity is within the range reported to activate cones in mice(Nathan et al. 2006; Umino et al. 2008).

The second situation invokes a saturating nonlinearity between rods and rod bipolar cells, as well as a threshold nonlinearity between cones and cone bipolar cells. This model could also account for the first two observations listed above. However the last two observations are hard to reconcile with this interpretation. The measured decrease in the sustained part of the rod bipolar cell's response suggests that rod response decreases when the light level is stepped to the critical level. Furthermore, if we assume that it is not the activation of cones that leads to the stepwise increase in cone bipolar responses then we expect to find a second major increase in the responses of cone bipolar cells when cones are activated at a higher light levels. However our recordings do not show such an increase.

Based on these observations, together with a pervious finding that rod-cone coupling in mice is weak during the day when our recordings were performed(Ribelayga et al. 2008), we favor the explanation that the stepwise increase in cone bipolar responses, which leads to switch-ON state, is due to the activation of cones.

In our view rod activity provides, through the rod-rod bipolar and possibly the rod-cone coupling pathways(Bloomfield & Dacheux 2001), a constant level of activation at the light levels around the switch. This constant activation together with the addition of cone activity enables the combined drive to reach the threshold of amacrine cells. When connexin36 is not present, rod activity does not contribute to the activity of cone bipolar terminals. This may explain the reduced PV1 cell spiking activity at the critical

intensity in connexin36 knock out animals. The relative weight of the different rod pathways, which is different in different species(Protti et al. 2005) as well as during day and night(Ribelayga et al. 2008) has likely little influence on the switch since these pathways converge at the cone bipolar terminals.

As one moves from dim to bright environments adaptive mechanisms in the retina play an active role in enabling vision to continuously function. These mechanisms include adaptive changes in specific synaptic and cell signaling pathways, and have been shown to regulate retinal sensitivity depending on the light level(Fain et al. 2001; Green & Powers 1982; Ichinose & Lukasiewicz 2007; Shapley & Enroth-Cugell 1984). One form of adaptation is the luminance dependent changes in electrical coupling between specific cell types including horizontal cells, AII amacrine cells, and ganglion cells(Bloomfield & Völgyi 2004; De Vries & Schwartz 1989; Hu et al. 2010; Mangel & Dowling 1985; Ribelayga et al. 2008; Xin & Bloomfield 1999). Many of these luminance dependent changes have been associated with light dependent changes in dopamine release in the retina(Lasater 1987; Mills & Massey 1995; Witkovsky 2004). We found no role for dopamine in effecting the switch of spatial integration properties of the PV1 cell. Instead, we show that the surround of PV1 cells is dependent on the presence of electrical coupling mediated by connexin36. The results of the connexin36 knock-out and pharmacology experiments in this work, together with a previous finding that some ON cone bipolar cells express connexin36(Siegert et al. 2012) suggest that some ON cone bipolar cells are electrically coupled to amacrine cells other than just AII(Deans et al. 2002). Our data are consistent with the implementation of a circuit switch that uses a threshold mechanism to turn on and off the antagonistic surround of PV1 cells depending on the strength of the stimulus. Although the proposed circuitry incorporates electrical coupling, it does not rely on adaptive mechanisms affecting the strength of the electrical coupling.

The Relationship between the Retinal and Perceptual Switch

The luminance effects on visual perception of spatial patterns show the same trends in mice, humans, cats, and monkeys(De Valois et al. 1974; Kelly

1972; Pasternak & Merigann 1981; Umino et al. 2008; Van Nes et al. 1967). With increasing stimulus luminance, contrast sensitivity at each spatial frequency increases, while peak sensitivity and acuity shift towards higher spatial frequencies. In addition, the relative sensitivity to low spatial frequencies decreases with increasing stimulus intensity(Barlow 1958; De Valois et al. 1974; Pasternak & Merigann 1981; Umino et al. 2008; Van Nes et al. 1967). While our study agrees with previous reports in regard to the continuous increase in peak sensitivity and acuity, we noted a discontinuous change in the preference for medium over low spatial frequencies. This discontinuity occurred at the same light level as the ability to discriminate color and, therefore, at the threshold of cones.

There are similarities between the luminance-dependent changes in the contrast sensitivity of observers and the neuronal responses of the cells in retina. In particular, the corresponding changes in shape of the contrast sensitivity functions of retinal ganglion cells(Bisti et al. 1977; Dedek et al. 2008; Enroth-cugell & Robson 1966) and perception(De Valois et al. 1974; Pasternak & Merigann 1981; Umino et al. 2008; Van Nes et al. 1967). Visual spatial processing is thought to be organized into a series of parallel, independent channels where each is tuned to a different spatial frequency(Blakemore et al. 1969; Watson et al. 1983). In the retina we found that large, but not small, ganglion cells showed changes in receptive field structure at the critical light level. This could explain the discontinuous increase in contrast sensitivity at low spatial frequencies if these low frequency channels start specifically with large ganglion cells.

Potential Benefits of the Switch

In dim environments it is necessary to gather as many photons as possible in order to *detect* objects of interest, while in bright condition one needs to *discriminate* between objects from the flood of thousands to millions of photons. We found that the change in spatial integration properties occurs only in select ganglion cell types, and occurs over a small luminance change. In light of these findings we ask why do large ganglion cell types lose their

antagonistic surround, and what benefit might the switch-like change in receptive field structure convey?

We showed that the luminance dependent changes in the organization of the receptive fields of two large cells (PV1 and PV6) switched at a critical light level, while that of two smaller cells (PV0 and PV2) did not. For some cells the loss of inhibitory input would eliminate the fundamental response properties that define their function. For example, direction selective ganglion cells are unable to discriminate direction when their inhibitory inputs are blocked(Caldwell et al. 1978; Fried et al. 2002). For small ganglion cells with center-surround receptive fields, an increase in integration area may not be a significant advantage. However, ganglion cells with large receptive field areas are well designed to detect objects when the photon count is low (low acuity, high sensitivity). For large cells, a loss of antagonistic surround would increase the area from which they could gather photons, as well as increase the overlap between neighboring receptive fields. Interestingly, one type of faintly melanopsin positive cell, M4, has a morphology that is similar to PV1 cells(Ecker et al. 2010; Estevez et al. 2012). If the two cell types are indeed the same, an intriguing possibility is that during evolution, a class of melanopsin cells acquired input from a special type of wide-field amacrine cell which conferred to it new spatial processing properties.

The loss of antagonistic surround may have benefits both for the individual cell, as well as for the mosaic as a whole. By increasing the area from which an individual cell can gather photons these cells become more sensitive to photons arriving within their receptive field. In addition, it has been demonstrated that broad overlapping receptive fields can be advantageous(Seung & Sompolinsky 1993), particularly when extracting information from sparse natural scenes containing large blank spaces of uniform contrast(Cuntz et al. 2007).

The contrast sensitivity of the rod pathways is thought to be lower than that of the cone pathway. This leads to a sparser encoding of the visual scene in low light levels forming contiguous blank neuronal representations in the rod pathways. An increased overlap between neighboring cells' receptive fields would allow the ganglion cell mosaic to interpolate between neighboring

high contrast features. This difference in contrast sensitivity between rod and cone pathways may explain why the transition between the two circuit states is switch like and not continuous.

We found that the change in spatial integration properties of PV1 cells occurs over a small luminance change (0.07 log unit), as compared to the more than 3 log unit range of intensities typical of many natural scenes(Geisler 2008; Mante et al. 2005; Rieke & Rudd 2009). In addition, the spatial integration properties of the PV1 cell could be toggled quickly as the light level was switched above and below the threshold light level. The circuit we propose would allow each ganglion cell of a single mosaic to individually set their spatial integration properties instantaneously, depending on the local luminance level of the scene. This would contribute to increasing the dynamic range of this mosaic by increasing integration in areas of low luminance and discrimination in areas of high luminance.

Experimental Procedures

Animals

Mice used in our experiments included Pvalb^{Cre} × Thy$^{Stp-EYFP}$, Pvalb^{Cre} × Ai9, Pvalb^{Cre} × Ai3 and mice in which the Cx36$^{-/-}$ alleles were crossed into Pvalb^{Cre}× Thy$^{Stp-EYFP}$ so that PV1 cells were labeled in a homozygous Cx36$^{-/-}$ background. In Pvalb^{Cre} mice(Hippenmeyer et al. 2005), Cre recombinase is expressed under the control of the parvalbumin locus. In Thy$^{Stp-EYFP}$ mice(Feng et al. 2000), EYFP is expressed from a Thy1 promoter in those cells in which the transcriptional stop sequence has been removed by Cre recombinase. In Ai3 and Ai9 mice(Madisen et al. 2010), ZsGreen or tdTomato is expressed from the CAG promoter in those cells where the transcriptional stop sequence has been removed by Cre recombination. Cx36$^{-/-}$ mice are homozygous knockouts for the electrical synapse protein connexin36(Deans & Paul 2001). All animal procedures were performed in accordance with standard ethical guidelines (European Communities Guidelines on the Care and Use of Laboratory Animals, 86/609/EEC) and were approved by the Veterinary Department of the Canton of Basel-Stadt.

Preparation of Retinas

Retinas were isolated from mice that had been dark-adapted for 2 hours. Retina isolation was done under infrared illumination in Ringer's medium (110 mM NaCl, 2.5 mM KCl, 1 mM CaCl$_2$, 1.6 mM MgCl$_2$, 10 mM D-glucose, 22 mM NaHCO$_3$, bubbled with 5% CO$_2$/95% O$_2$, pH 7.4). The retinas were then mounted ganglion cell-side up on filter paper (Millipore) that had a four mm wide rectangular aperture in the center, and superfused in Ringer's medium at 35–36°C in the microscope chamber for the duration of the experiment. The infrared light used for dissection had its peak power at 850 nm (Figure S2). This resulted in an effective absorption by rods of 0.05 photons absorbed per rod per second (R*/s). Red LED head lamps, with a peak power of 650 nm were used to navigate around the room, and at a distance of 10 cm caused an effective absorption of 1.21 R*/s (Figure S2).

Electrophysiology and Pharmacology

Electrophysiological recordings were made using an Axon Multiclamp 700B amplifier (Molecular Devices) and borosilicate glass electrodes (Sutter Instrument). Signals were digitized at 10 kHz (National Instruments) and acquired using software written in LabVIEW (National Instruments). Data were analyzed offline using MATLAB (MathWorks).

The spiking responses were recorded using the patch clamp technique in loose cell-attached mode with electrodes pulled to between three and five MW resistance and filled with Ringer's medium.

Current recordings were made in whole-cell voltage clamp mode, with electrodes pulled to between five and eight MW resistance and filled with 112.5 mM $CsCH_3SO_3$, 1 mM $MgSO_4$, 7.8×10^{-3} mM $CaCl_2$, 0.5 mM BAPTA, 10 mM HEPES, 4 mM $ATP-Na_2$, 0.5 mM $GTP-Na_3$, 5 mM lidocaine N-ethyl bromide (QX314-Br), 7.5 mM neurobiotin chloride. The pH was adjusted to 7.2 with CsOH. The reversal potential for chloride (E_{Cl}) was calculated to be ~ -60 mV. 13 mV was subtracted from all voltages to correct for the disappearance of the liquid junction potential upon establishing the whole-cell recording. Series resistances of between 10 and 25 MW were corrected for offline. Excitatory currents were recorded while holding cell at -60 mV and inhibitory currents were recorded while clamping the cell at 0 mV.

Voltage recordings were made in whole-cell current clamp mode, with electrodes pulled to between five and eight MW resistance and filled with 115 mM K gluconate, 1.95 mM KCl, 1 mM $MgCl_2.6H_2O$, 0.5 mM $CaCl_2$, 1.5 mM EGTA, 10 mM HEPES, 4 mM $ATP-Na_2$, 0.5 mM $GTP-Na_3$ and 7.5 mM neurobiotin chloride. In order to visualize the neurons, in some experiments, either Alexa Fluor 488 or 594 was added to the intracellular solution listed above.

In pharmacological experiments, agents were bath-applied at the following concentrations: 10 mM CPP, 10 mM NBQX, 10 mM APB, 10 mM strychnine, 100 mM picrotoxin. All chemicals were obtained from Sigma-Aldrich, with the exception of APB (Calbiochem), ATP (Labforce), neurobiotin (Vector Laboratories) and Alexa Fluor 488 and 594 (Molecular Probes).

Bipolar Cell Recordings

Retinas were mounted ganglion-cell down on filter paper (Millipore). 200 μm thick slices were prepared using a tissue chopper (Stoelting) under infrared illumination. Slices were transferred into a custom-made recording chamber. Bipolar cells were recorded in whole cell voltage clamp configuration, at -60 mV.

Analysis of Physiological Data

The firing rate of a neuron was calculated by convolving spike trains with a Gaussian kernel with a standard deviation of 25 ms. During voltage clamp recordings, excitatory and inhibitory synaptic currents were separated by voltage clamping the cell to the equilibrium potential of chloride (-60 mV), and unselective cation channels (0 mV), respectively. Only recordings with a series resistance between 10 and 25 MW were used. For voltage clamp recordings, the response to a light stimulus (Figure 1.4D and E, Figure 1.6D, E and F) was calculated by taking the mean current during the first 0.5 s after stimulus onset. The early excitatory responses (Figure 1.6I and J) were calculated by taking the mean current between 50 and 150 ms after stimulus onset.

The spatial integration properties of ganglion cells were evaluated either by comparing their spiking response during the presentation of a spot with the size of the individual cell type's dendritic field (400 mm for PV1 and PV6 cells; 250 mm for PV2 cells), and the response during the presentation of a spot of 1000 mm such that:

$$\text{spatial selectivity index (SSI)} = \frac{\text{Response}_{\text{Small}} - \text{Response}_{\text{Large}}}{\text{Response}_{\text{Small}} + \text{Response}_{\text{Large}}}$$

Where the Response was defined as the number of spikes during stimulation. Response is a variable that takes non-negative integers, or, during the presentation of drifting gratings, the SSI was calculated by comparing the magnitude of the first harmonic (F1) of the spike frequency

response to drifting grating with a temporal frequency of 0.5 Hz and spatial wavelength of either 500 or 4000 um such that:

$$\text{SSI} = \frac{\text{F1}_{500} - \text{F1}_{4000}}{\text{F1}_{500} + \text{F1}_{4000}}$$

Where F1 was calculated by computing the Fourier transform of the spike frequency, and determining the magnitude of the Fourier transform at the temporal frequency of the stimulus. The Fourier transform was calculated using the fast Fourier algorithm in Matlab.

The direction selectivity of a ganglion cell was quantified as the vector sum of the spiking response (number of spikes) of the cell to a bar moving in eight different directions. The Direction Selectivity Index (DSI) is defined as:

$$\text{DSI} = \sum_{d} \frac{\overrightarrow{N_d}}{R_d}$$

where N_d are vectors pointing in the direction of the stimulus and have a length of R_d.

Targeted Recordings using Two-Photon Microscopy

Fluorescent cells were targeted for recording using a two-photon microscope equipped with a Mai Tai HP two-photon laser (Spectra Physics) integrated into the electrophysiological setup (Figure S3). To facilitate targeting, two-photon fluorescent images were overlaid on the IR image acquired through the CCD camera. Infrared light was produced using the light from a projector equipped with a digital light processor (DLP) and a 750 +/- 25 nm filter. The resulting light absorbed by the retina corresponded to 0.11 R*/s (Figure S2). In order to target PV1 cells in Pvalb^{Cre} × Thy$^{Stp-EYFP}$ and Pvalb^{Cre} × Ai9 we used two anatomical criteria, the size of the cell body and the stratification of the dendrites. In the Pvalb^{Cre} mouse line we find three cell types labeled with large cell bodies of >20 mm. Of these, one has dendrites that stratify in the ON lamina. Specifically, the dendrites of the PV1 cell lie between the ganglion cell layer and the proximal dendrites of ON-OFF direction selective cells (PV0). The two strata where the dendrites of ON-OFF direction selective cells stratify were brightly labeled in the Pvalb^{Cre} × Thy$^{Stp-EYFP}$ and Pvalb^{Cre} × Ai9 mice. Among the PV cells, PV1 is the only one that

arborizes between the proximal dendritic trees of ON-OFF direction selective cells and the ganglion cell layer.

In order to target other cell types in these mouse lines, an image stack was obtained with the two-photon microscope previous to patch-clamp recording. The cells were then targeted based on the size of their cell body and the characteristic morphology of their dendritic trees. The monostratified cells are named in the order in which their dendritic trees terminate in the inner plexiform layer, where the PV1 cells arborize closest to the ganglion cell layer and PV6 cells closest to the inner nuclear layer. PV2 stratified distal to the proximal PV0 labeled strata. See a detailed description of the physiology and morphology of all PV cells in Figure 2 and S1, respectively.

Visual Stimulation

Stimuli were generated with a DLP projector (PLUS) at a refresh rate of 75 Hz, controlled with custom software written in MATLAB. The projector produced a light spectrum (Figure S2) that ranged from ~400 nm to ~720 nm. The power produced by the projector was 229 mW/cm^2 at the retina (Figure S2). Neutral density filters were used to control the stimulus intensity in logarithmic steps. This allowed us to maintain constant contrast at each light level. We calculated contrast as the Michelson contrast:

$$\text{Contrast}_{\text{Michelson}} = \frac{\text{Luminance}_{\text{max}} - \text{Luminance}_{\text{min}}}{\text{Luminance}_{\text{max}} + \text{Luminance}_{\text{min}}}.$$

For spot stimulations the Michelson contrast was 0.9993, at each light intensity. In all experiments using a spot stimulus the contrast was kept constant, we only changed the mean illumination by neutral density filters. The light intensity of the stimulus, rather than the background, is shown on the figures. The reason for this is that there are conditions when the background is below cone threshold but the stimulus is above cone threshold, and since the switch is instantaneous, this stimulus turns on the switch. When grating stimuli are used the maximum intensity of the grating is shown for the same reason. We express light intensity in photoisomerizations per rod per second (R*/s). Light intensity was measured with a photodiode power meter (Thorlabs), and the spectrum was measured with a spectrometer (Ocean

Optics). The photoisomerization rate was computed based on the absorption spectrum of the photoreceptors(Lyubarsky et al. 1999), and a collecting area of 0.5 mm^2 for rods and 0.2 mm^2 for cones(Nikonov et al. 2005; Nikonov et al. 2006). The range of light intensities present at the retinal surface, ranged from 0.006 to 1.03 × 10^7 R*/s (Figure S2). This range covers the reported ranges of rod and cone visual function in mice(Nathan et al. 2006; Field et al. 2005; Umino et al. 2008).

White noise stimuli consisted of a central spot and 8 concentric annuli that were independently assigned a random luminance value each frame, which was drawn from a Gaussian probability distribution with a mean intensity and a standard deviation, such that the Michelson contrast was 0.25. The central spot was 200 mm in diameter. The concentric annuli had inner diameters of 200, 400, 600, 800, 1000, 1200, 1400 and 1600 mm and were each 200 mm thick. The stimulus consisted of 7500 frames and was shown at a frame rate of 15 Hz.

Classification and Types of Ganglion Cells in PV Mice.

In Pvalb^{Cre}× Thy$^{Stp-EYFP}$ mice we encountered eight morphological types of ganglion cells (Figure S1). These are named PV0-PV7.
Quantitative morphological classification was based on the depth of dendrites in the inner plexiform layer using the ChAT marked strata as rulers (0 and 100%) and the area occupied by the dendrites(Manookin et al. 2008; Münch et al. 2009). See Figure S1 for quantitative definition of morphological types. Qualitatively, PV0 cells were bistratified costratifying with the ChAT strata. The rest of cells were monostratified. Proximal from the proximal-ChAT strata are PV1 cells. Just distal from the proximal-ChAT strata are PV2 cells. In between the two ChAT strata are PV3 cells. Just proximal from the distal ChAT strata are the PV4 and PV5 cells. PV4 cells have smaller dendritic area than PV5 cells. PV6 and PV 7 cells are distal from the distal ChAT strata. PV7 cells have smaller dendritic area than PV6 cells.

Confocal Analysis

Stained retinas were imaged with a Zeiss LSM 700 confocal microscope. Filled ganglion cells were imaged using a 20x air (NA 0.7) and, a 40x oil immersion (NA 1.2) lens. The mCherry-labeled circuits of PV-positive ganglion cells were imaged with a Zeiss LSM 710 confocal microscope using a 63x (NA 1.4) oil immersion lens. Reconstructions of neurons were made in Neurolucida (MBF Bioscience) and TrackEM2 (ImageJ).

Monosynaptically Restricted Circuit Tracing

Two different strategies were used to achieve monosynaptic restriction of virus infection, one used a combination of G-deleted rabies virus encoding mCherry (SADΔG-mCherry) with conditional, rabiesG-expressing replication-defective herpes simplex virus-1 (HSV1); the second used a conditional, rabiesG-expressing adeno-associated virus (AAV) instead of the HSV1 (Figure S6).

G-deleted rabies virus encoding mCherry (Marshel et al., 2010) was supplied by E. Callaway. Rabies virus was harvested from BHK-B19G cells (provided by E. Callaway) and centrifuged(Wickersham et al. 2010).

To create HSV1-EF1a-LoxP-STOP-LoxP-G-2A-EGFP, the EGFP open reading frame (ORF) in the HSV1 vector pR19EF1a-EGFP-WCm (Biovex) was replaced with a sequence of loxP-STOP-loxP followed by the ORF of rabiesG-2A-EGFP. First, the sequence of LoxP sites and G-2A-EGFP ORF was synthesized (DNA2.0) with a combination of EcoRI-BsrGI restriction sites in the extremities. The sequence of rabiesG was taken from pHCMV-RabiesG(Sena-Esteves et al. 2004). The EGFP ORF was removed from pR19EF1a-EGFP-WCm by EcoRI/BsrGI digestion and the synthesized fragment of LoxP-STOP-LoxP-G-2A-EGFP was subcloned into the EcoRI–BsrGI site.

Recombinant AAVs (serotype 7, BIOVEX) were made from a backbone of the vector AAV-EF1a double floxed-hChR2(H134R)-EYFP-WPRE-hGHpA (provided by K. Deisseroth), using the NheI-AscI site; the ChR2 and EYFP

ORF was substituted by the ORF of rabiesG taken from pHCMV-RabiesG(Sena-Esteves et al. 2004) using an in-fusion PCR kit (TAKARA). Titer determination was made using real-time PCR (titer: 5.78×10^{12} genome copies per ml, determined using real-time PCR).

In the herpes/rabies combination strategy we performed stereotaxic surgery in Pvalb^{Cre} × Thy1$^{Stp\text{-}EYFP}$ or Pvalb^{Cre} × Ai3 mice to label ganglion cells projecting to the superior colliculus and the lateral geniculate nucleus (LGN). A cocktail of 10^3 plaque-forming units of rabies virus and 6×10^4 plaque-forming units of HSV1 in 20 nl Dulbecco's modified eagle medium (DMEM) were loaded into pulled-glass pipettes (tip inner diameter of 20–30 mm) and injected into the superior colliculus or LGN using a microinjector (Narishige). Note that LGN infection resulted in many more PV1 cells. In the second strategy AAV particles (1.5µl, 8.68×10^9 GC) were loaded into pulled glass pipettes and injected into the vitreal space of both eyes of Pvalb^{Cre} × Thy1$^{Stp\text{-}EYFP}$ or Pvalb^{Cre} × Ai3 mice. Six days later 10^3 plaque-forming units of rabies virus was injected into the superior colliculus or the LGN to label ganglion cells projecting to them. Again, LGN infection yielded many more PV1 cells. All rabies, AAV and HSV1 work was carried out under Biosafety level 2 conditions.

The goal of these experiments was to initiate retrograde passage of rabies from PV ganglion cells. Since the conditional AAV or herpes viruses only express rabiesG in Cre-positive ganglion cells, only this subset of ganglion cells are able to infect pre-synaptically connected cells.

The morphological characterization of wide-field amacrine cells specifically connected to PV1 cell, takes ~1 month for each PV1 cell and we reconstructed three examples of PV1 circuits. With the current tracing protocol (Herpes + rabies from Cre cells, or AAV + rabies from Cre cells), the probability of virus transsynaptic transfer from adult ganglion cells is low, therefore one encounters a number of PV1 cells that are rabies infected but the rabies did not pass to any of the circuit elements.

The practical limitation for reconstructing ganglion-wide-field cell circuits is that the processes of wide-field cells are thin and long (>1 mm) and therefore neither large field/low numerical aperture (NA) nor small field/high NA objectives are capable of capturing the processes of the wide-field cells. In

searching for connectivity between wide-field and PV1 cells we performed the following four steps.

The first step was to create a large, stitched 3D image stack that was big enough to capture the PV1 and the wide-field cells (Figure S7). We created a 3D reconstruction of a 2.08 × 2.08 mm piece of retina around a PV1 cell, by creating 144 confocal image stacks with 10% overlap that tile the 2.08 × 2.08 mm retinal space. Each stack has x=1024, y=1024, z=215 pixels, where the size of the z step is 330 nm and the x and y pixel width is 188 nm. The objective has 63x magnification and 1.4 NA. We then stitched these stacks together to create a single 3D digital image of the selected piece of retina (11060 × 11060 × 215 pixels). We scanned through every PV1 dendrite to look for thin processes that contacted the dendrites. We identified contact points.

The second step was to confirm each contact point at a higher resolution. We created 3D reconstruction areas around each contact point at higher resolution (see Figure 5 B-D). The x and y pixel widths for this higher resolution were 27 nm and the z step was 166 nm. The size of the digital stack was 2048 × 2048 × 45 pixels.

The third step was the reconstruction of the morphology of the PV1-conneted cells. We went back to the original large image stack and traced every cellular process that contacted the PV1 ganglion cell dendrite back to their cell bodies, and then we further traced all the processes that emerged from those cell bodies. Using this procedure we obtained the image as shown in Figure 5A.

The fourth step, which was key to showing connection specificity, was to check if any of the amacrine cells connected to PV1 cells may also contact other PV cells. We walked through all the processes of the PV1-connected amacrine cells to look for connectivity to other PV cells. We accepted that an amacrine cell was specifically connected to PV1 cells if it did not contact any other PV cells. Note that with our current tracing protocol this final step is, in practice, only feasible for displaced amacrine cells connected to PV1 cells (note that the wide-field cells we found connected to PV1 cells were displaced cells) and for amacrine cells which had cell bodies in the inner nuclear layer that were connected to PV6 or PV7 cells. The reason for this is the following:

PV1 dendrites occupy the most proximal strata of all PV cells (see Figure S1). If a displaced wide-field amacrine cells is connected to a PV1 cell, it does not cross strata where other PV cell dendrites arborize, and therefore it is relatively easy to rule out connections to other PV cells. The same argument holds for PV6- or PV7-connected amacrine cells that have cell bodies in the inner nuclear layer, since PV6 and PV7 cell dendrites occupy the most distal strata among all PV cells. For other selected PV cells, such as PV3 for example, the processes of both displaced and non-displaced amacrine cells have to pass through strata, which are populated by labeled dendrites of PV cells, which are not PV3. Ruling out connection of an amacrine process to ganglion dendrites as they pass through a retinal layer is only feasible in a few cases.

Immunohistochemistry

After the experiments, the retinas were fixed for 30 min in 4% paraformaldehyde in PBS (137 mM NaCl, 2.7 mM KCl, 4.3 mM Na_2HPO_4, and 1.47 mM KH_2PO_4, pH7.4), then washed in PBS for a minimum of one day at 4°C. To aid penetration of the antibodies, retinas were frozen and thawed three times after cryoprotection with 30% sucrose. All other procedures were carried out at room temperature. After washing in PBS, retinas were blocked for 60 minutes in 10% normal donkey serum (NDS), 1% bovine serum albumin (BSA), and 0.5% Triton X-100 in PBS. Primary antibodies were incubated for seven days in 3% NDS, 1% BSA, 0.02% sodium azide and 0.5% Triton X-100 in PBS. Secondary antibodies were incubated for 90 minutes in 3% NDS, 1% BSA, 0.02% sodium azide and 0.5% Triton X-100, in PBS. After a final wash in PBS, retinas were embedded in ProLong Gold Antifade (Molecular Probes).

The following set of primary and secondary antibody combinations were used in experiments in which we recorded from PV-positive ganglion cells labeled with tdTomato from the Ai9 reporter line. Primary: goat anti-ChAT and rabbit anti-red fluorescent protein (Millipore). Secondary: donkey anti-goat IgG conjugated with Alexa Fluor 633; donkey anti-rabbit IgG conjugated with Cy3 (Jackson ImmunoResearch Laboratories, PA);

streptavidin-Alexa Fluor 488 and 4',6-diamidine-2-phenylindole dihydrochloride (DAPI, Roche Diagnostics). Rabbit anti-red primary antibody binds to tdTomato.

The following set of primary and secondary antibodies combinations were used in experiments in which we recorded from PV ganglion cells labeled with EYFP from the Thy1$^{Stp-EYFP}$ line. Primary: goat anti-ChAT, and rat anti-GFP (Nacalai Tesque). Secondary: donkey anti-goat IgG conjugated with Alexa Fluor 633; donkey anti-rat IgG conjugated with Alexa Fluor 488; streptavidin-Alexa Fluor 568 and DAPI. Rat anti-GFP also binds EYFP.

The following set of primary and secondary antibodies combinations were used in experiments in which we recorded from PV ganglion cells labeled with ZsGreen from the Ai3 reporter line. ZsGreen was bright enough to detect cell bodies without antibody labeling. Primary: goat anti-ChAT. Secondary: donkey anti-goat IgG conjugated with Alexa Fluor 633; streptavidin-Alexa Fluor 568 and DAPI.

The following set of primary and secondary antibodies combinations were used for staining mCherry expressing rabies virus-infected retinas. Primary: goat anti-ChAT, rabbit anti-RFP and rat anti-GFP. Secondary: donkey anti-goat IgG conjugated with Alexa Fluor 633, donkey anti-rabbit IgG conjugated with Cy3 and donkey anti-rat IgG conjugated with Alexa Fluor 488. Rabbit anti-RFP also binds to mCherry.

Psychophysical Experiments

In order to assess the spatial integration properties of human vision at different light levels we measured the contrast sensitivity function (CSF) of human volunteers at five different light levels after a period of two hours of dark adaptation. To measure the CSF of each volunteer we determined the minimum contrast at which a Gaussian-windowed vertical sinusoidal grating could be detected. This is reported as contrast sensitivity (1/threshold). We repeated this test at spatial frequencies of 0.45, 1.14, 2.80, 4.60, 11.40, 22.80, and 45.60 cycles per degree (cpd) at mean luminance levels of 0.002, 0.02, 0.2, 2.0 and 22 cd/m^2.

The sine wave images were projected onto a screen with an LCD projector (Epson EH-TW3200) with a refresh rate of 60 Hz and a bit depth of 10 bits for each colour. The projector was enclosed in a light tight box and neutral density filters (Thorlabs) were used to control the brightness of the projected images in logarithmic steps. Stimuli were viewed binocularly with natural pupil at a viewing distance of three meters. The images were rendered on a 1280 × 1028 pixel grid, extending 43.6 × 35° of visual angle. The background luminance was set to the middle of the dynamic range of the display. For the CSF trials 30 possible gratings contrasts were spaced log-linearly from 0.1 to 99.5%. The stimulus sequence began with the presentation of the lowest contrast sinusoidal grating of a particular spatial wavelength. Subjects controlled custom-built software, written in Python, which allowed them to step through the different contrasts and determine their own contrast sensitivity for each grating presented. 11 naive observers and five of the authors participated in the experiment. All observers had corrected-to-normal vision. The human spatial selectivity index (hSSI) was defined as the ratio between the contrast sensitivity at the lowest spatial frequency and the peak contrast sensitivity:

$$\text{hSSI} = \frac{\text{Sensitivity}_{\text{Peak}} - \text{Sensitivity}_{\text{Low}}}{\text{Sensitivity}_{\text{Peak}} + \text{Sensitivity}_{\text{Low}}}$$

The colour discrimination task consisted of a forced choice paradigm, where volunteers were presented two rectangles, one red the other blue, and had to decide which one was red. Each red, blue pair was pseudo randomly selected from a set of five hues of red and five hues of blue. This task was repeated 50 times at each light level.

Model of Switch Circuitry

The model of the switch circuitry consisted of three basic building blocks: the cone bipolar cell terminal (CBT); the switch cell (SC); and the PV1 ganglion cell (PV1). Inputs to the CBT were the weighted light responses of the recorded rod and ON-cone bipolar cells at different background light intensities (Figure 6), and the feedback signal from the SC. The SC was driven by the CBT. The CBT-SC loop was modeled as a coupled differential

equation, which controlled the state of CBT and SC. The states CBT and SC were rectified to produce the output of CBT and SC. The bend of the state-output curve was shifted to the right in SC to model spike threshold (Figure S8).

1. $\dot{x}(t) = -x(t) + \mathrm{Wrb}\, \mathrm{rb}(t) + \mathrm{Wcb}\, \mathrm{cb}(t) - \mathrm{Wyx}\, H(y(t) - \mathrm{Tsc})(y(t) - \mathrm{Tsc})$

2. $\dot{y}(t) = -y(t) + \mathrm{Wxy}\, H\big(x(t)\big)\, x(t)$

Where x(t) represents the state of CBT, Wrb and Wcb are the gains associated with the rod and cone bipolar input, respectively, Wyx is the feedback gain from SC, Tsc models the spike threshold of SC, H is the Heaviside step function, y(t) represents the state of SC and Wxy is the gain of the excitatory input from CBT to SC.

The weighted (We) CBT output was the time varying excitatory conductance, ge(t), of PV1,

3. $\mathrm{ge}(t) = \mathrm{We}\; H\big(x(t)\big)\, x(t)$

The weighted (Wi) SC output was the time varying inhibitory conductance, gi(t), of PV1,

4. $\mathrm{gi}(t) = \mathrm{Wi}\; H(y(t) - \mathrm{Tsc})(y(t) - \mathrm{Tsc})$

The membrane potential of the PV1 cell was integrated using the membrane equation:

5. $-C\,\dot{V}(t) = g\,(V(t) - \mathrm{Vr}) + \mathrm{ge}(t)\,(V(t) - \mathrm{Ve}) + \mathrm{gi}(t)\,(V(t) - \mathrm{Vi})$

where g, PV1 membrane conductance in rest, C, PV1 membrane capacitance, and Vr, resting membrane voltage (~-50 mV), were measured (Figure S8). Ve, reversal potential of excitatory currents, was set to 0 mV and Vi, reversal potential for inhibitory currents, was set to -60-70 mV. The spikes were generated from the membrane voltage signal, at membrane depolarization, using a Poisson process. Since Vr was close to PV1 spike threshold, spikes were initiated even by small membrane depolarization. The free parameters of the model were the gains of the sign preserving and sign inverting pathways (Figure S8) and the threshold of SC. These parameters were fitted to match the recorded inhibitory, excitatory and spiking responses (see comment at the end of this paragraph about relative weight of inhibition and excitation). The model simulated the responses to two different-sized spots. The first, 400 mm in diameter, covered the entire dendritic field of the

ganglion cell and so maximized its excitatory input. The second, 1000 mm in diameter, was larger than the dendritic field of the ganglion cells. The gains of the sign preserving synapses were kept the same for both stimuli. To model wide-field inhibition from SC, the gains of sign inverting, inhibitory, pathways were different between the two stimuli. The difference between these inhibitory gains was determined by fitting the model's inhibitory conductance to PV1 to the recorded inhibitory conductance evoked by the two stimuli. Note that the experimentally recorded excitatory input to PV1 cells was faster than the inhibitory input (Figure 5F), resulting in few spikes at the onset of the 1000 mm stimulus at daylight conditions (Figure 1A and S4). Model showed similar delay. The delay in the model was caused by the spike threshold of SC. The magnitude of delay was dictated by time course of the bipolar cell responses since this was the slowest component of the system.

In order for inhibitory conductance to achieve the measured reduction in spiking frequency at cone threshold, it has to be ~3 times larger than excitatory conductance. This is, because during an unclamped voltage response the driving force of inhibition is ~3 times less than for excitation. Yet, as shown on Figure 5D, the mean inhibition in the first 500 ms after stimulus onset has smaller magnitude than excitation (both measured with the same driving force). There are two reasons for this discrepancy. First, the time course of inhibition and excitation is not the same. Excitation starts with a large transient followed by a smaller sustained component. Inhibition has a similar peak transient, but is delayed compared to excitation (Figure 5C and 5F). The initial large excitatory peak causes a few spikes at stimulus onset (Figure 1A and S4). However, when inhibition is reaching its maximum excitation is already falling and therefore inhibition is larger than excitation. This explains that transient hyperpolarization after the few spikes following stimulus onset. Second, as far as the reduction of spiking in the sustained component of the response, the magnitude of inhibition is likely underestimated in our voltage clamp experiments. When recording inhibitory input we voltage clamp the cell at 0 mV, far from the resting potential. For large cells, such as PV1 cells, this results in space clamp at distal dendrites and the recorded current is a combination of inhibitory outward and excitatory inward current with a net outward current. Therefore the magnitude of the

recorded outward current underestimates the current component caused by the inhibitory input. Simulations were carried out in Mathematica.

Statistical Analysis

All measures of statistical difference were performed using a Mann-Whitney U test. In the figures, statistical significant difference is indicated with *, **, or ***, representing P values less than 0.05, 0.01 and 0.001, respectively. All data points are mean +/- s.e.m. The "n" in the figures refers to the number of different cells from which recordings were used for the actual figure, or in the case of human experiments the number of individuals.

A. *Pvalb^{Cre} × Thy^{Stp-EYFP}* retina
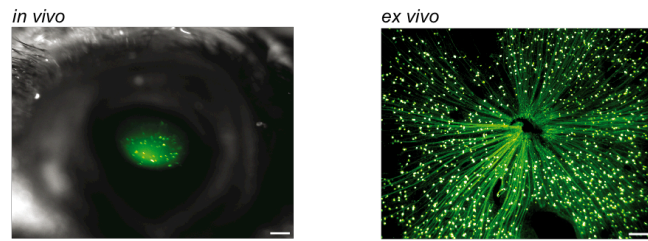
B. Morphology of PV cells
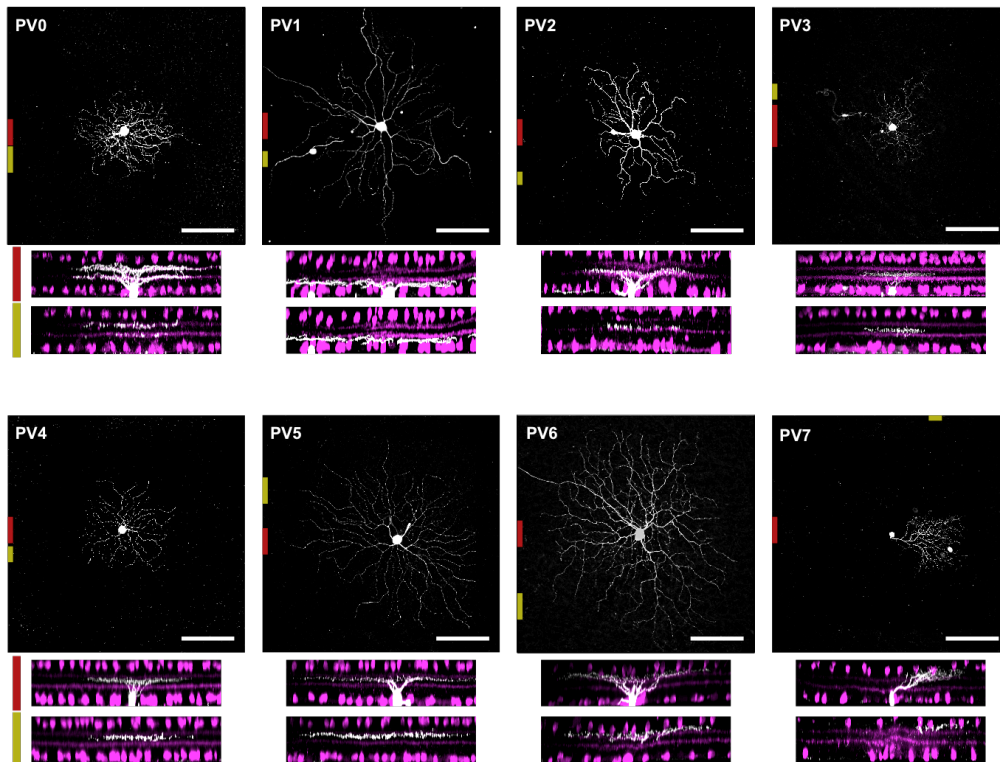
C. Quantification of morphology
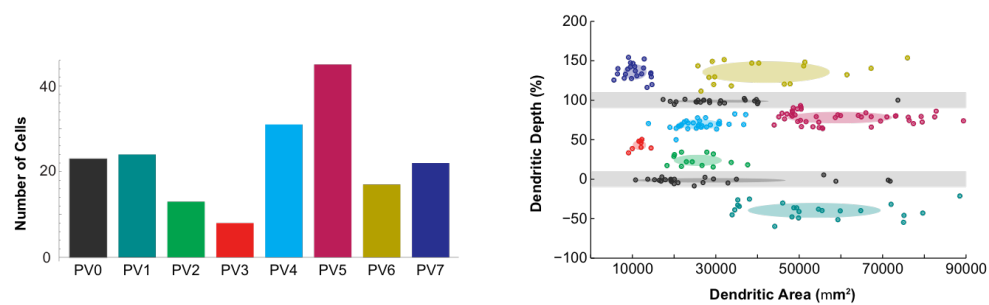
Figure S1. Morphology of PV ganglion cells.

A. Left, in vivo fluorescent image of the eye of a Pvalb^{Cre} X ThyStp-^{EYFP} mouse. Right, ex vivo fluorescent image of a whole mount retina from the same mouse line. B. Examples of morphologies of PV cells from each PV cell type. Top panels show maximum image projections of confocal image stacks of neurobiotin filled cells. The two bottom panels show side views highlighting the stratification of

dendrites. (dendrites, white; ChAT cells, magenta). Red and yellow lines indicate the position and range within the stack. **C**. *Quantification of the morphology. Left, histogram of the number of confocal microscopy reconstructed cells of each type in our data set. Right, scatter plot of each cell's dendritic stratification in the inner plexiform layer versus dendritic area. The depth of dendritic stratification was determined using a procedure described before*(Münch et al. 2009). *Each shaded ellipse spans one standard deviation along each axis. The proximal and distal ChAT bands are defined as 0% and 100% depth.*
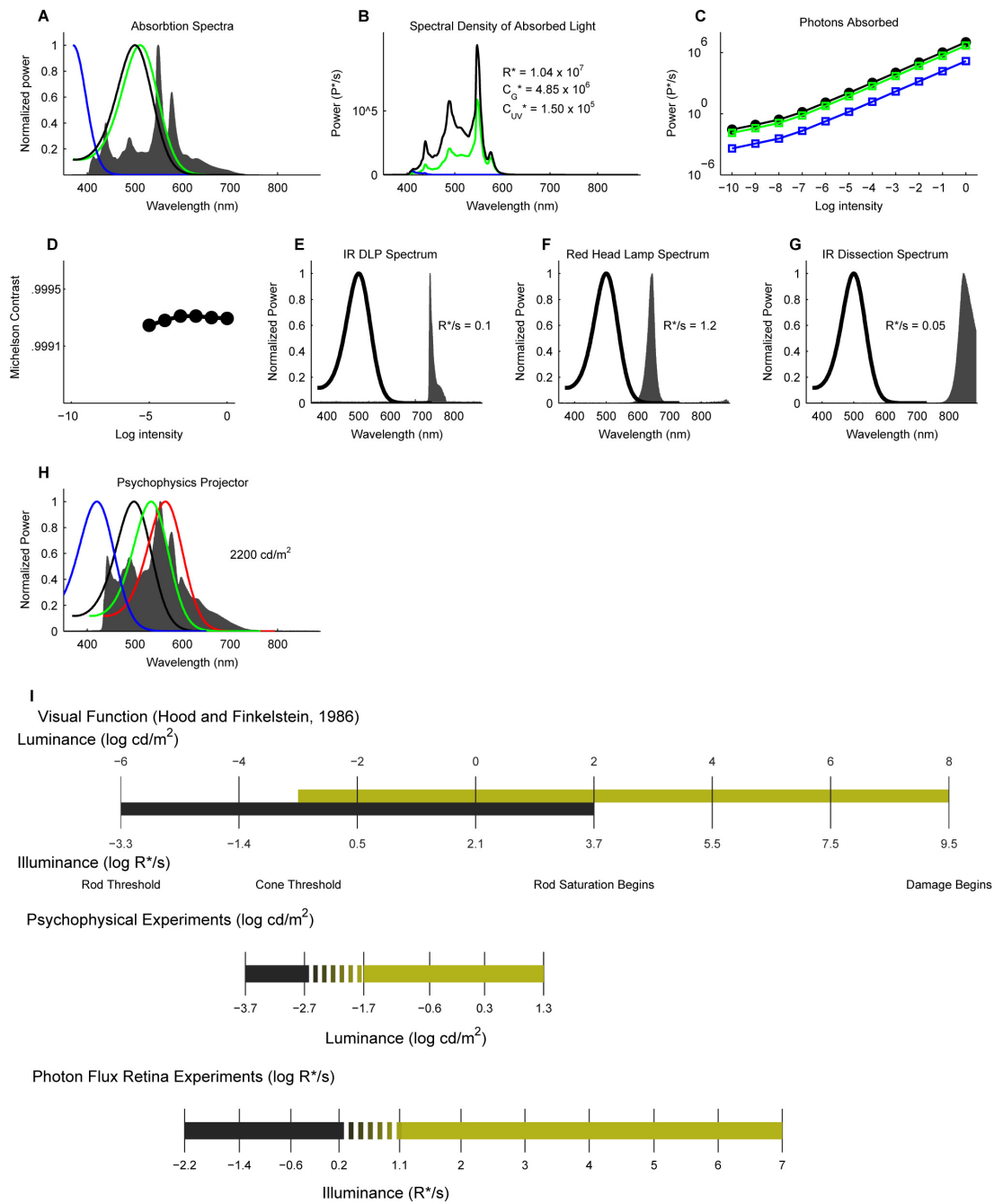
Figure S2. Quantification of stimulus parameters.

A. Normalized emission spectrum of the DLP projector (filled black) used for mouse retina experiments overlaid on the normalized absorption spectra of mouse photoreceptors (black: rod; green: green cone; blue: UV cone). **B.** Spectrum of absorbed light for each photoreceptor type. **C.** Number of photons per photoreceptor absorbed by each photoreceptor type at the different light levels. **D.** Contrast of the stimulus measured across different light levels. The Michelson contrast was 0.9993. **E-G.** The normalized absorption spectrum of rods is overlaid with the emission spectrum of infrared illumination used to visualize cells during experiments (**E**); to

*navigate around setup (**F**), and to dissect the retina (**G**). These three light sources caused a maximum illumination corresponding to 0.1, 1.2 and 0.05 R*/s. **H.** Spectrum of DLP projector (filled black) used for human psychophysics experiments overlaid on absorption spectra of human photoreceptors (black: rod; blue: blue cone; green: green cone; red: red cone). **I.** Comparison of light levels used in our experiments for humans and mice with the light levels used by Hood and Finkelstein (1986) for quantifying human visual performance. Black: light levels when rods are operational; yellow: when cones are operational.*

A

2P Excitation
Fluorescent Emission
DLP Illumination

Camera

2P Laser

PMT

Objective 60x, NA = 0.8

Filter wheel

Condenser, NA = 0.8

DLP Projector

B

IR Camera

IR filter

IR Filter: 750 +/- 25 nm

Dichroic

Dichroic: 400 - 815 band pass

Blocking filter
380 - 680 nm band pass

IR blocking

Dichroic

Dichroic: 700 long pass

Filter wheel

IR filter (750 +/- 25 nm): cell visualization
or
ND filters: visual stimulation

Illumination from DLP projector

C 2P image of EYFP cells

D 2P image of filled PV1 cell

E

Z-projection of filled PV1 cell

***Figure S3 Light pathways for visual stimulation, two-photon imaging, and IR visualization.***

***A**, **B**. Layout of the two-photon microscope. **A** ~920 nm laser line (red line) from a Mai Tai HP twophoton laser (Newport) was attenuated using polarization optics (Newport) and a Pockels cell (Conoptics, Model 302), and was scanned using mirrors (Cambridge Technologies) mounted on a modified Olympus microscope. The*

*fluorescent signal emitted (green line) was detected with a photo multiplier tube (Hammamatsu, R3896). An infrared camera (Diagnostic Instruments, Spot RT) mounted on the microscope allowed the visualization of the retina during two-photon scanning. To visualize neurons labeled with fluorescent proteins or dyes the retina was illuminated through the condenser with IR light using a DLP projector (V332, PLUS) filtered with an infrared filter (750 +/- 25 nm; Chroma) while simultaneously recording the two-photon fluorescent images. The IR image and scanned two-photon image were fused for visualization. **C.** Maximum intensity top projection of a two-photon image stack showing EYFP-expressing cells in PvalbCre Å~ ThyStp-EYFP retina. Top (**D**) and z-projection (**E**) of a two-photon stack of images showing an Alexa594 dye-filled PV1 cell. Scale bar on C-E 25 mm.*

A. Summary of flashing spot experiments
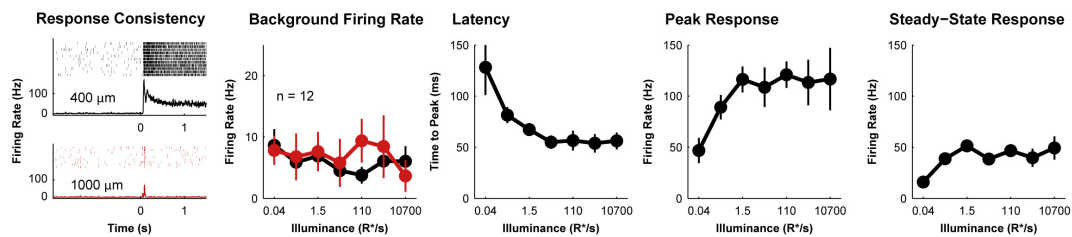
B. Summary of drifting grating experiments
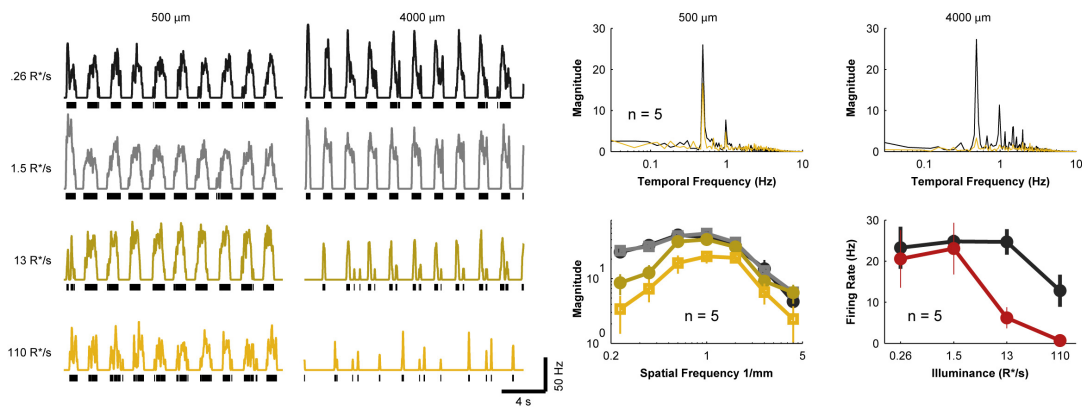
C. Summary of white noise experiments

Figure S4. Summary of PV1 cell responses in dark and light.

A. *Summary of PV1 spiking responses. For response consistency the mean firing rate and the individual raster plots from a single experiment are shown. For the bac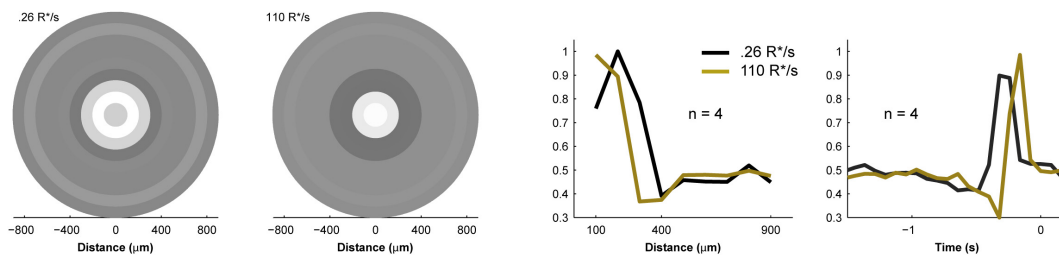kground firing rate, latency, peak response and steady-state response the average across all experiments are shown. For background firing rate red is 1000 mm spot, and black represents 400 mm spot. Latency, peak response and steady-state responses refer to 400 mm spot stimulations. Data is plotted as mean +/- sem.*
B. *Summary of drifting grating experiments. Left, example of response of PV1 cell to drifting grating with a contrast of 0.4 and spatial wavelength of either 500 or 4000 mm. Continuous lines show the spike frequency of response. Vertical lines are recorded spikes. Right top, Fourier transform of responses to drifting gratings. Black curves are responses at .26 R*/s. Yellow curves responses at 110 R*/s. Right bottom, contrast sensitivity function of PV1 cell (left). Mean firing during presentation of 500 (black) or 4000 (red) mm gratings (right).* ***C.*** *Summary of spatio-temporal white noise experiments. Left, spatial profile of spike triggered average (STA) of PV1 cell at 0.26 R*/s. and at 110 R*/s. Right, STA of PV1 cells at 0.26 R*/s (black) and 110 R*/s (yellow), spatial profile and time course are shown.*
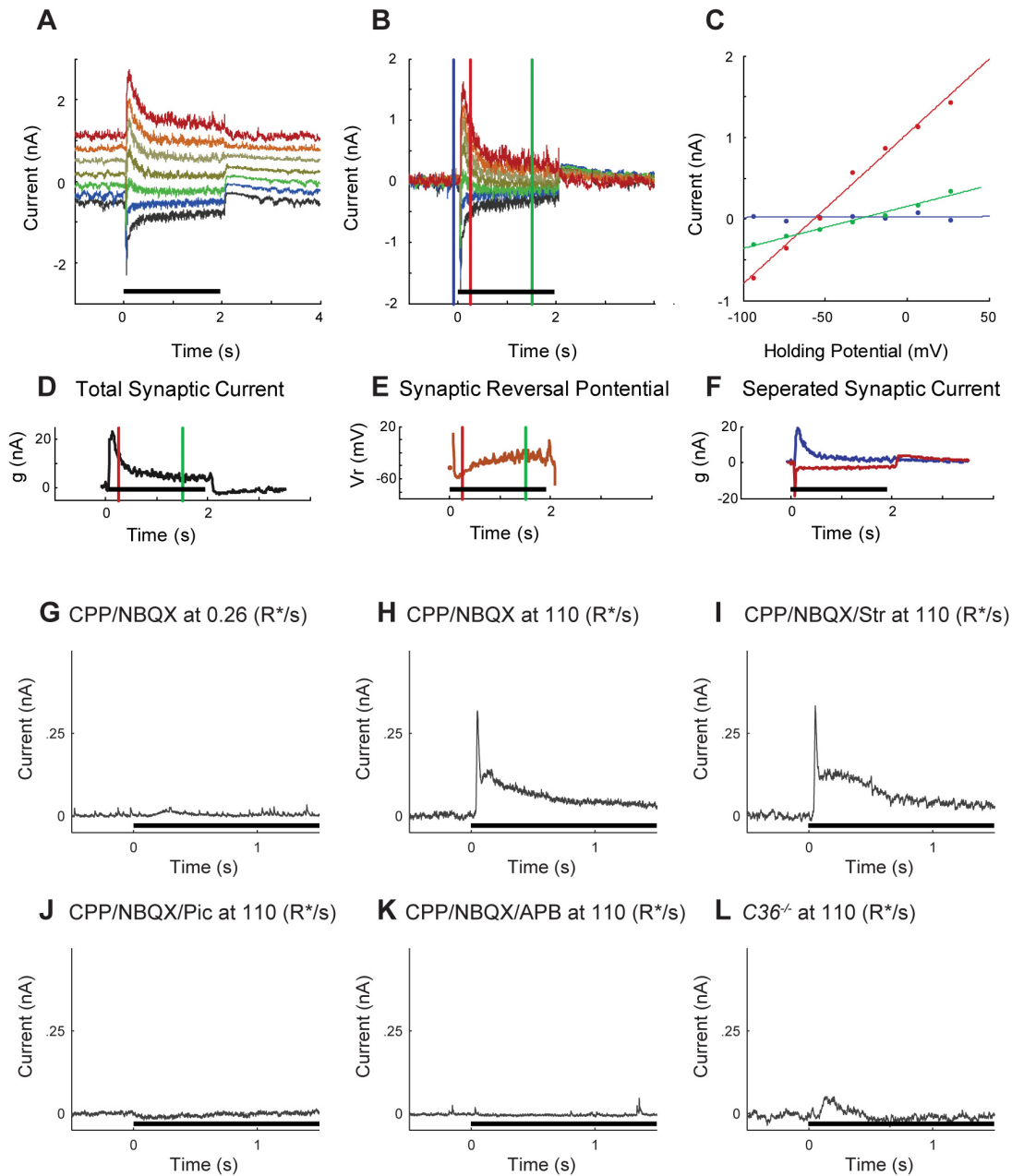
Figure S5. Voltage clamp analysis and examples of PV1 cell inhibitory current traces.

A. Current recorded before, during and after the presentation of a spot while clamping the membrane potential of the neuron at different potentials. The light level was 110 R*/s. B. The pre-stimulus current is subtracted from the curves on A. Three time points are indicated by the colored lines. C. Currents from B are linearly fitted at three time-points during the light-response. The colors correspond to the time points indicated by vertical lines of the same color in B. D. The slope of the fitted lines at each time point, representing the stimulus-evoked conductance (g). E. The x-intercept of the fitted lines at each time point, representing the reversal potential (Vr).

*F. Based on the inhibitory and excitatory reversal potentials of -60 and 0 mV, respectively, the inhibitory and excitatory conductances are separated. In G-L the stimulus was a 1000 mm spot presented at time zero, the first 1.5 s of the response is shown. Each trace is the average of 3 individual presentation of the stimulus from a single recording session. **G.** The inhibitory current recorded in the presence of CPP and NBQX at a light level of corresponding with the switch-OFF state of 0.26 R*/s. **H.** The inhibitory current recorded in the presence of CPP and NBQX at a light level of corresponding with the switch-ON state of 110 R*/s. **I.** The inhibitory current recorded in the presence of CPP, NBQX and Strychnine (Str) at a light level of corresponding with the switch-ON state of 110 R*/s. **J.** The inhibitory current recorded in the presence of CPP, NBQX and Picrotoxin (Pic) at a light level of corresponding with the switch-ON state of 110 R*/s. **K**. The inhibitory current recorded in the presence of CPP, NBQX and APB at a light level of corresponding with the switch-ON state of 110 R*/s. **L.** The inhibitory current recorded in a connexin36 knock out mouse (Cx36$^{-/-}$) at a light level of corresponding with the switch-ON state of 110 R*/s.*

A

Floxed AA-G strategy

Injected floxed G - expressing AAV

Injected G-deleted rabies encoding mCherry

Floxed herpes-G strategy

Co-injected G-deleted rabies encoding mCherry &
floxed-G expressing herpes

Eye

Retina

Optic nerve

LGN

V1

superior
colliculus

Eye

Retina

Optic nerve

LGN

V1

superior
colliculus

B

EYFP

G-deleted rabies mCherry

EYFP + G-deleted rabies mCherry

EYPF + G-deleted rabies mCherry +
floxed-AAV-G or floxed-herpes-G

C

PV1

A1

PV1

A1

PV1

A1

Figure S6. Monosynaptically restricted viral tracing strategies.

A. *Strategy 1 (left): G-deleted rabies virus is injected into either the LGN or the superior colliculus (two different projection sites of retinal ganglion cells), while the floxed-AAV (which conditionally expresses G) is injected into the eye where it can infect retinal ganglion cells directly. Strategy 2 (right): G-deleted rabies virus and floxed-herpes virus (which conditionally expresses G) are co-injected into either the LGN or superior colliculus. **B**. We performed all viral tracing experiments in the PvalbCre Å~ ThyStp EYFP or PvalbCre Å~ Ai3 mice, where a subset of ganglion cells are labeled green (left panel). If G-deleted rabies expressing a red fluorescent protein is used in a wild-type mouse we see red-labeled ganglion cells (center left panel). If G-deleted rabies is used in a PvalbCre Å~ ThyStp-EYFP or PvalbCre Å~ Ai3 mouse we see some ganglion cells labeled both green and red, here indicated as yellow (center right panel). If G is also 11 provided via either floxed-AAV or*

61

floxed-Herpes, we see yellow ganglion cells as well as red-labeled presynaptic amacrine cells. **C.** *Example of transsynaptic tracing of PV1 cells. Maximum image projections of confocal stacks are shown. Left, green channel (Ai3 is the reporter mouse here) shows PV cell bodies. Middle, red channel showing rabies infected cells. Right, overlay of the two channels. Note that the PV1 cell is labeled by both mCherry from rabies and ZsGreen from the Ai3 mouse line, while the connected amacrine cell, A1, is only labeled by mCherry. Note that the processes of the amacrine cells are too thin to be visible at this scale. Scale bar is 50 mm.*
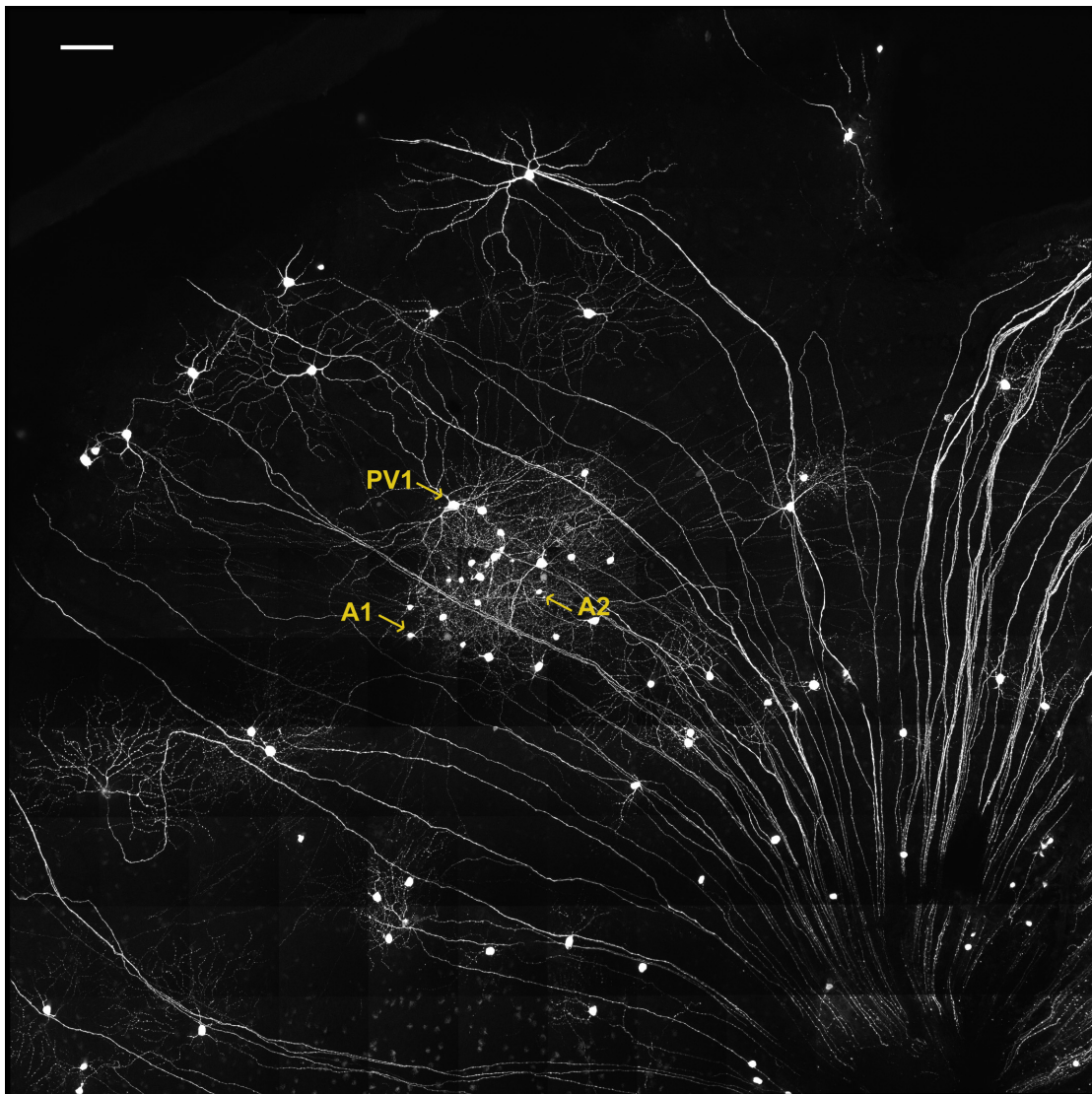
Figure S7. Overview image in a viral tracing experiment.

Maximum image projection of stitched confocal stacks used to trace connections from an example PV1 cell. The red channel, showing red fluorescent protein expressed by rabies is displayed. The image is flattened from 144 stitched image stacks. A PV1 cell and two connected amacrine cells are highlighted. The processes of amacrine cells are only faintly visible at this scale. Scale bar is 100 mm.
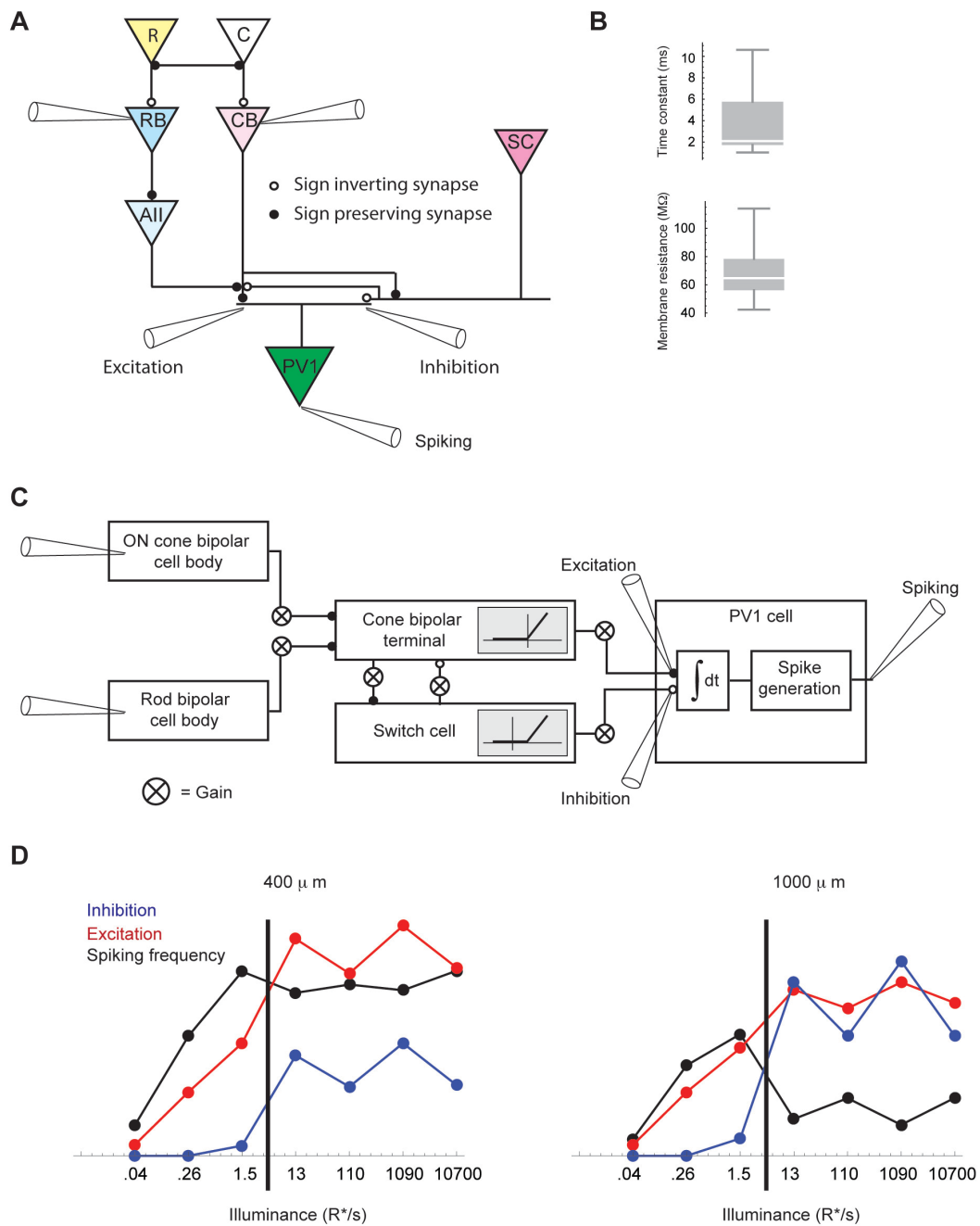
Figure S8. Model of the switch circuit.

 A. Cell types in the circuit of PV1 cells. Electrodes point at positions in the circuit where responses were recorded. B. Time constant and membrane resistance of PV1 cells. C. Building blocks of the model. D. The predictions of the model. The model is described in Experimental Procedures. Each point corresponds to the mean response of the first 500 ms after stimulus onset.

## Chapter 2 – Slow Contrast adaptation in specific parvalbumin-positive ganglion cells

Introduction

Slow contrast adaptation can be divided into two different processes in ganglion cells, one occurring over the receptive field center and another in the periphery of the receptive field(Demb 2008). Slow contrast adaptation over the receptive field center is thought to be caused by a prolonged membrane after-hyperpolarization that suppresses firing(Baccus & Meister 2002). Experiments made show that current injections that evoked depolarization and spiking were not enough to produce the same amount of membrane after-hyperpolarization than the one visually evoked(Manookin & Demb 2006). Slow contrast adaptation over the receptive field periphery of ganglion cells could be partially explained by synaptic inhibition on two different sites in the retina, the direct inhibition of ganglion cells dendrites by synaptic inhibition through wide-field amacrine cells(Zaghloul et al. 2007) and inhibition on presynaptic bipolar cell terminals(Zaghloul et al. 2007). In order to identify the mechanism present that is responsible for slow adaptation in the retina, we first observed the response of a specific subset of retinal ganglion cell types, parvalbumin positive neurons.

Results

I performed targeted loose cell patch 2-photon imaging to 7 different types of parvalbumin-positive ganglion cells and stimulated them with a stimulus previously used by Smirnakis et al in 1997(Smirnakis et al. 1997). This stimulus consists of a random Gaussian distribution of different intensities. New stimulus intensity was chosen every 33 ms from a Gaussian probability distribution with mean intensity M and standard deviation W. Contrast, defined as W/M, was 0.35 for high-contrast flicker, and 0.05 for low-contrast flicker (figure 2.1). By keeping the mean light intensity constant

throughout the experiment contributions from adaptation to light intensity were avoided.
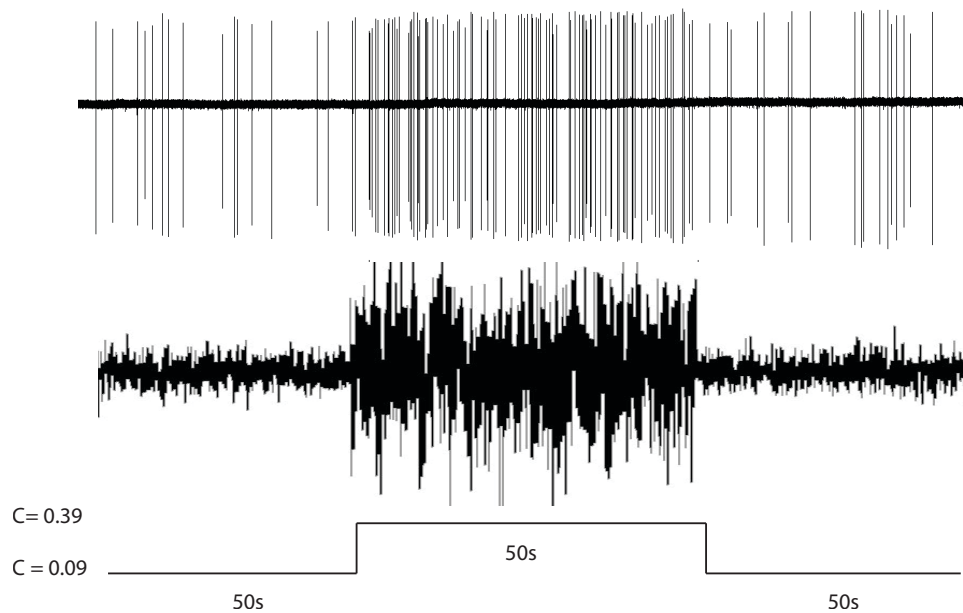
Figure 2.1. Stimulus used for eliciting contrast adaptation.
Ganglion cell firing elicit by a 275 um spot, on a grey background, where its intensity was chosen every 33 ms at random from a random Gaussian probability distribuition with mean M and standard deviation W. Contrast C, was defined by W/M. The middle trace represents the randomness of the intensy of the spot. The bottom trace illustrates the time course of the flickering intensity of the spot, with each step of contrast change being 50 s.

Ganglion cell type differentiation was not observed but we noticed a subclass division in the response to a contrast change stimulus. Some cells types showed a decrease in spiking frequency quickly after contrast change while others either maintain their spike frequency or decrease in the beginning but climb again to the average. PV0, an ON-OFF direction-selective cell when submitted to the contrast adaptation stimulus showed an increase in firing rate when the higher contrast started and then had a decay for the first 25 seconds of high contrast, slowly stabilizing at a plateau and even increasing its firing rate in the last seconds of high contrast. PV1 an On alpha cell, showed an increase in firing rate when the high contrast stimulus was initiated but slowly

showed a stable decay during the high contrast step of the stimulus. PV2, an On transient cell in response to the stimulation responded with an big increase in firing rate after the change to high contrast followed by a sharp decrease in the first 5 seconds and a steady decay until the end of the high contrast stage of the stimulation. PV4, an OFF-transient cell, after the initial increase of firing rate show a decay for a short period of time and then return to the maximum firing rate observed. PV5, the approaching-motion cell, showed the normal increase after high contrast but had a very small decay in firing rate. PV6, an OFF sustained cell, show a small increase in firing rate after the change to high contrast maintaining it in a stable level until the change to low contrast. PV7, the well known GAMbH cell, increases slightly after change in contrast and also maintains its level constant until the change to low contrast. Three different cells responded to the contrast adaptation stimulus with a decay of their spiking response (figure 2.2), PV0 and PV2 responded in a two step kinetics, with a sharp decrease of response in the first 10 seconds and then reached a plateau, the third cell type, PV1, responded with a continuous decrease of its spiking response. Although PV0 is an ON-OFF cell, the characteristic that joins these cell types together is that fact that they are all types that responds to increments of light.

Interestingly the other cell types studied were all cell types that did not adapt to contrast change and also were all types that respond to decrements of light (figure 2.3), PV4, PV5, PV6 and PV7 all responded with the same firing rate throughout the high contrast step of the stimulus not decreasing their response. PV4 initially shows some adaptation but its firing rate comes back to the average point after some minutes

This result gives an indication that the circuitry of cell that respond to decrements of light do not compute contrast adaptation as it was thought
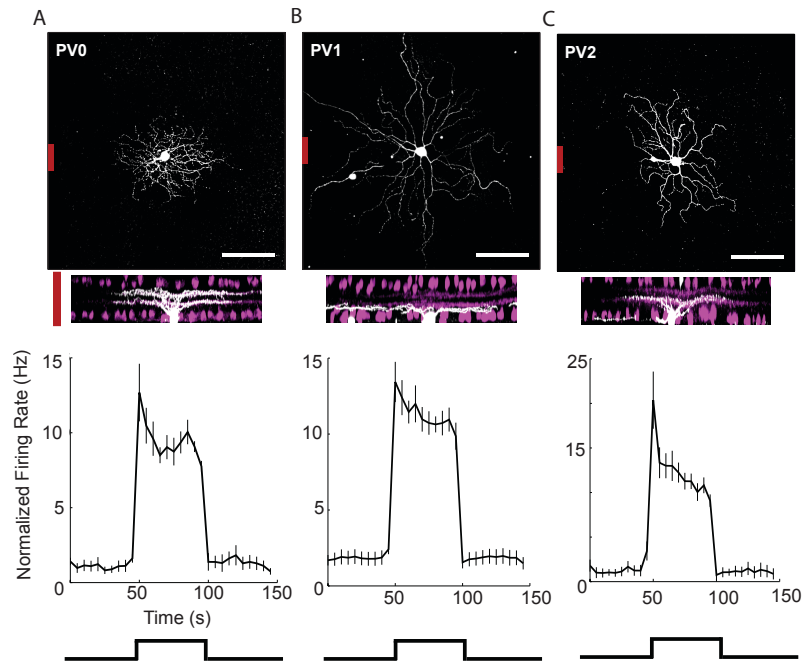
Figure 2.2 On cells adapt to changes in contrast.

*The morphology of PV0 (**A**), PV1 (**B**), PV2 (**C**) retinal ganglion cells are summarized. Top panels: top view of example PV cells. The scale bar represents 100 μm. Middle panels: z-projection (white) overlaid on an antibody staining of ChAT-expressing cells (magenta), which form two bands in the inner plexiform layer. on the bottom the normalized firing rate calculate on fixed bins of 5 s in the duration of the stimulus, five cells of each class were observed and each cell was shown between 25 to 30 stimulus continuously. PV0 is an ON-OFF direction selective cell adapts well to a change in contrast. PV1, which is a large ON cell, also adapts to a increase in contrast change with a steady decrease of the firing rate. PV2, which is a small On cell, has a biphasic adaptation, with a very fast decline of the firing rate followed by a steady decrease. Error bars were standard error of the mean (s.e.m)*
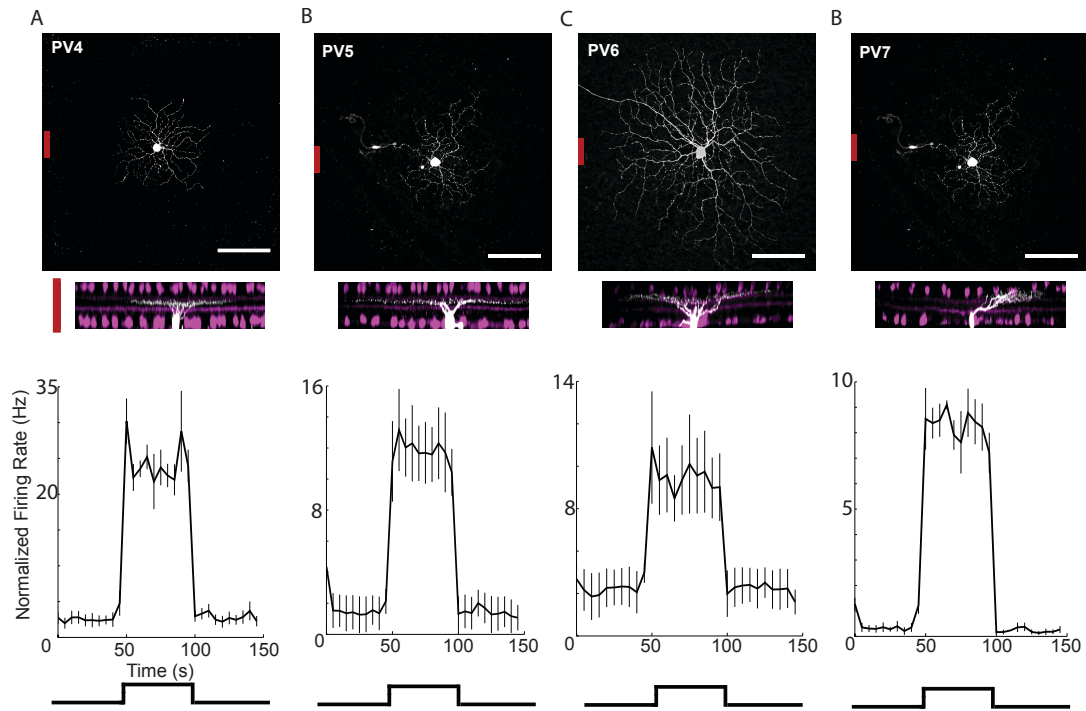
Figure 2.3. Off cells do not show adaptation.

*The morphology of PV4 (**A**), PV5 (**B**), PV6 (**C**) and PV7 (**D**) retinal ganglion cells are shown. Top panels: top view of example of each PV cells. The scale bar represents 100 μm. Middle panels: z-projection (white) overlaid on an antibody staining of ChAT-expressing cells (magenta), which form two bands in the inner plexiform layer. In the bottom panels, normalized firing rate of each PV Off cell is plotted, fixed bins of 5 s, versus the time of the stimulation, all plots comprise of 5 cells each, only the PV7 only has only four cells recorded. The four off cells present on this mouse line do not show much adaptation to the change to higher contrast. Error bars are s.e.m.*

Experimental Procedures

Animals

Mice used in our experiments included Pvalb^{Cre} × Thy$^{Stp-EYFP}$, Pvalb^{Cre} . In Pvalb^{Cre} mice[19], Cre recombinase is expressed under the control of the parvalbumin locus. In Thy$^{Stp-EYFP}$ mice[21], EYFP is expressed from a Thy1 promoter in those cells in which the transcriptional stop sequence has been removed by Cre recombinase.. All animal procedures were performed in

accordance with standard ethical guidelines (European Communities Guidelines on the Care and Use of Laboratory Animals, 86/609/EEC) and were approved by the Veterinary Department of the Canton of Basel-Stadt.

Preparation of retinas.

Retinas were isolated from mice. Retina isolation was done under infrared illumination in Ringer's medium (110 mM NaCl, 2.5 mM KCl, 1 mM $CaCl_2$, 1.6 mM $MgCl_2$, 10 mM D-glucose, 22 mM $NaHCO_3$, bubbled with 5% CO_2/95% O_2, pH 7.4). The retinas were then mounted ganglion cell-side up on filter paper (Millipore, MA) that had a four - five mm diameter rectangular aperture in the centre, and superfused in Ringer's medium at 35–36°C in the microscope chamber for the duration of the experiment.

Electrophysiology.

Electrophysiological recordings were made using an Axon Multiclamp 700B amplifier (Molecular Devices) and borosilicate glass electrodes (Sutter Instrument). Signals were digitized at 10 kHz (National Instruments) and acquired using custom software written in LabVIEW (National Instruments). Data were analyzed offline using MATLAB (MathWorks) and Python (The Python software foundation). The spiking responses were recorded using the patch clamp technique in loose cell-attached mode with electrodes pulled to between three and five MW resistance and filled with Ringer's medium.

Immunohistochemistry.

After the experiments, the retinas were fixed for 30 min in 4% paraformaldehyde in PBS (137 mM NaCl, 2.7 mM KCl, 4.3 mM Na_2HPO_4, and 1.47 mM KH_2PO_4, pH7.4), then washed in PBS for a minimum of one day at 4°C. To aid penetration of the antibodies, retinas were frozen and thawed three times after cryoprotection with 30% sucrose. All other procedures were carried out at room temperature. After washing in PBS, retinas were blocked for 60 minutes in 10% normal donkey serum (NDS), 1% bovine serum

albumin (BSA), and 0.5% Triton X-100 in PBS. Primary antibodies were incubated for seven days in 3% NDS, 1% BSA, 0.02% sodium azide and 0.5% Triton X-100 in PBS. Secondary antibodies were incubated for 90 minutes in 3% NDS, 1% BSA, 0.02% sodium azide and 0.5% Triton X-100, in PBS. After a final wash in PBS, retinas were embedded in ProLong Gold Antifade (Molecular Probes).

Confocal analysis.

Stained retinas were imaged with a Zeiss LSM 700 confocal microscope. Filled ganglion cells were imaged using a 20x air (NA 0.7) and, a 40x oil immersion (NA 1.2) lens. The mCherry-labeled circuits of PV-positive ganglion cells were imaged with a Zeiss LSM 710 confocal microscope using a 63x (NA 1.4) oil immersion lens. All reconstructions of neurons were made in Neurolucida (MBF Bioscience).

Chapter 3 – A nanobody-based system using fluorescent proteins as scaffolds for cell-specific gene manipulation.

Introduction

Studies of multi-cellular organisms would be greatly facilitated by the ability to manipulate the activities of genes within any tissue or cell type. This is challenging to achieve in tissues with diverse cell types, such as the nervous system (Masland, 2004). To label and provide genetic access to diverse cell types, much effort has been devoted to generating transgenic organisms in which transgenes are placed under the control of large genomic fragments or endogenous gene loci. Transgenic lines expressing driver genes such as transcription factors or site-specific recombinases can then be used to control the expression of genes in responder cassettes. However, the utility of individual lines is limited by a transgene's functional abilities; reporter lines expressing fluorescent proteins and histochemical enzymes are useful for labeling cells, but cannot currently be used to control biological activities. To replace transgenes driven by the same cis-regulatory elements requires generation of additional transgenic lines. Such a procedure can be costly and lengthy for organisms such as the mouse. Thus, a key to conducting efficient and wide-ranging studies on existing and future model organisms is to increase the versatility of transgenic resources.

Owing to their ease of detection, green fluorescent protein (GFP) and its derivatives(Tsien 1998) have become common markers of gene expression(Chalfie et al. 1997) across model organisms. Notably, thousands of transgenic GFP lines have been generated for the mouse(Gong et al. 2003). This growing and important resource reveals the expression pattern of many genes and provides strains in which GFP selectively labels many cell types of interest in the nervous system, particularly in the retina (www.gensat.org)(Siegert et al. 2009). Transgenic GFP lines have enabled

applications such as cell type-specific transcriptome profiling as well as targeted anatomical and physiological analysis(Huang et al. 2003)(Siegert et al. 2012). However, functional manipulation of GFP-labeled cell types often requires the use of driver lines such as those that express Cre, which currently exist in limited numbers.

A system converting GFP expression into desired molecular outputs would enable existing and future transgenic GFP lines to be used for gene manipulation of specific cell types. Intracellular proteins have previously been used to control gene expression with engineered RNA devices(Culler et al. 2010). While promising, these devices have yet to be applied in animals(Chang et al. 2012). Meanwhile, artificially-derived protein binders(Wurch et al. 2012) are being used to target proteins in cells and organisms, but thus far only for target-centric purposes such as protein interference(Jobling et al. 2003), degradation(Caussinus et al. 2012), and modulation(Kirchhofer et al. 2010). Artificial protein binders could possibly be a powerful platform to co-opt intracellular proteins as cell-specific signals that control synthetic circuits, without modifications to the target protein or reliance on the target protein's natural interactions or functions.

Results

One exciting use of T-DDOGs would be to express light-sensing ion channels in cell types labeled by transgenic GFP for refined, optogenetic probing of neural circuits(Yizhar et al. 2011).

We explored the possibility by using Tg(GUS8.4-GFP) to express a UAS-regulated channelrhodopsin-2 (ChR2) variant, H134R(Nagel et al. 2005) in GFP-labeled cells. We asked whether light-driven ChR2 activation in GFP-labeled bipolar cells could trigger downstream spiking responses in cells of the GCL (Figure 3.1D). Electroporated retinas were presented with two different light stimuli and recordings were performed on GCL cells. The first stimulus had low light intensity and could evoke photoreceptor-mediated responses in GCL cells, but was not bright enough to activate ChR2. We used

this stimulus to select GCL cells that responded to both light increments and decrements (ON/OFF cells) (Figure 3.1E-3.1F). We next blocked synaptic communication between photoreceptors and ON bipolar cells with 2-amino-4-phosphonobutyrate (APB) (Slaughter and Miller, 1981), and presented the retina with a brighter light stimulus that could activate ChR2. Since ON/OFF GCL cells receive excitatory input from ON bipolar cells, some of these cells should be connected via excitatory synapses (directly or indirectly) to ChR2-expressing ON bipolar cells. Indeed, the brighter stimulus elicited ON responses in some recorded GCL cells in the presence of APB (Figure 3.1G-6H). In contrast, recordings made from ON and ON/OFF GCL cells in non-electroporated regions of multiple retinas did not reveal any response after the onset of the brighter stimulus, in the presence of APB (data not shown). Thus, ChR2 activation in rod bipolar or ON cone bipolar cells was robust enough to evoke neurotransmitter release from bipolar cells. Further, the resulting current in GCL cells was large enough to reach spike threshold and evoke spiking responses. These results showed that T-DDOG could turn on optogenetic tools in transgenic GFP cells, permitting functional interrogation of neural circuits.
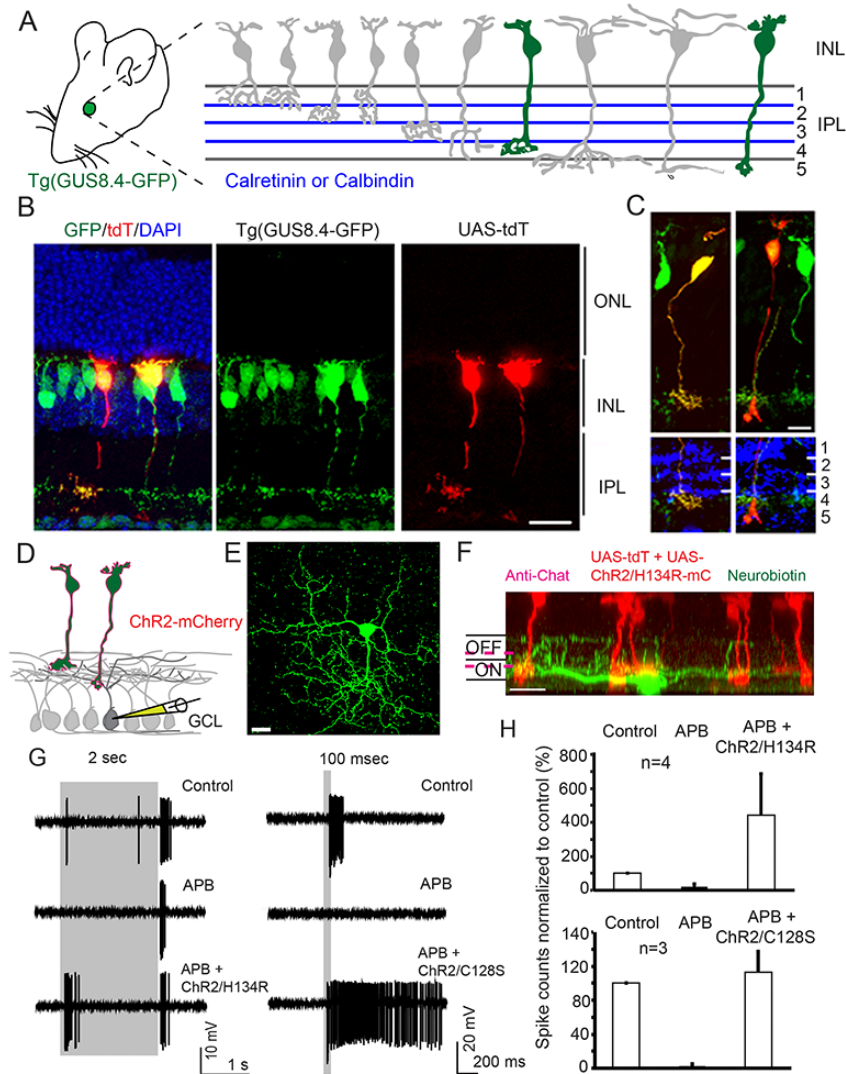
Figure 3.1. Retrofitting a transgenic GFP mouse line for GFP-dependent manipulation of gene expression and neural circuit activities.

(***A***) *Tg(GUS8.4GFP) expresses GFP in type 7 cone bipolar and rod bipolar cell types (green) of the retina. Adopted schematic (Ghosh et al., 2004).* (***B***) *Cryosection of electroporated, Tg(GUS8.4GFP) retina expressing Gal4-GBP2$^{p65\text{-}GBP7}$ and UAS-tdT. Scale bar, 20µm.* (***C***) *Type 7 (left) and rod bipolar (right) cell types labeled by UAS-tdT. Anti-Calretinin (left) or anti-Calbindin (right) stainings identify specific layers of the IPL. Scale bar, 10 µm. GFP was immunostained in (**B**, **C**).* (***D***) *Schematic of ChR2 experiment. Tg(GUS8.4-GFP) retinas expressing 10xUAS-ChR2/H134R-mCherry and5xUAS-tdT were analyzed for ChR2-mediated responses in random GCL cells.* (***E***) *Cumulative plot of ON responses in GCl cells. Number of spikes counted during the first 300 ms after stimulus onset, normalized to control (minus APB). APB blocks ON responses originating from photoreceptors. Plot is mean +/- SEM (n=4 per condition)* (***F***) *Spiking response of a GCL cell. Gray bar, duration of*

75

*light stimulus. Response to normal light stimuli under control condition (top), or in the presence of APB (middle). Light stimuli focused on INL activate ChR2/H134R in the presence of APB (lower). (**G** and **H**) top and side views of a nerobiotin-filled (green) ganglion cell identified by light stimulation of ChR2. Magenta lines indicate level of anti-Chat bands (not shown). Scale bar 20 μm*

Discussion

Fluorescent proteins are useful for illuminating cells and cellular processes. Moreover, their apparent lack of connection to many host protein networks makes them ideal scaffolds upon which one can build synthetic complexes with desirable biological activities. We demonstrated this principle here by using GFP to induce formation of a hybrid transcription factor for gene regulation purposes. The ability to use GFP for gene regulation now enables one to experiment with many GFP-labeled cell types without the need to create new cell-specific driver lines or to discover new cell-specific promoters. This system can be used for gene overexpression and gene deletion and should be able to perform RNA interference (RNAi) knockdown (Dickins et al., 2007; Dietzl et al., 2007). Activities of the system can be controlled by GFP and its derivatives, but not by red fluorescent proteins, thereby allowing the two types of fluorescent proteins to be used independently in the same experiment. Red fluorescent proteins can likely be used as scaffolds as well. In particular, monomeric variants such as mCherry would be straightforward to use, as they do not undergo obligate dimerization or tetramerization (Campbell et al., 2002).

Perspective on Targeting Intracellular Products for Cell-Specific Control

Many intracellular products, such as RNA and proteins, are expressed in a cell-specific manner and could potentially be exploited as spatial signals to control synthetic circuits in multicellular organisms. Here, we demonstrated that artificially derived binding proteins are useful for co-opting an intracellular protein, GFP, for this purpose. Because this approach does not require any modification of the target molecule or rely on the molecule's natural interactions or functions, it may be generalizable to any intracellular product for which artificially derived binding proteins can be selected. Certainly, GFP

seems to be an ideal target because it is an exogenous molecule that shows little connection to host protein networks. However, other exogenous molecules, such as β-galactosidase or Cre recombinase, should also be useful as scaffold proteins. Furthermore, endogenous molecules probably exhibit a spectrum of connectivity within the host interactome, and a subset might be appropriate for conferring cell-specific manipulations in multicellular organisms. The ability to use intracellular products simply as cell-specific scaffolds would enhance one's ability to target and control cells in non-model organisms where transgenic lines are not available.

Experimental Procedures

Neuronal recordings

For ChR2/H134R experiment, electroporated retinas from 8-10 weeks old Tg(GUS8.4GFP)-positive mice were flat-mounted, and loose cell-attached patch clamp was performed on GCL cells that had mCherry/tdT positive bipolar cells in their dendritic fields. 20 mM APB was used whenever applicable. Photoreceptors were stimulated by light focused on the outer segments of photoreceptors, at a light intensity of 1.3×10^3 R*/s. ChR2 was stimulated by light focused on the bipolar cell layer at ~10^8 R*/s for 2s. Detailed recording methods is provided in Extended

Electrophysiology and Pharmacology

Electrophysiological spike recordings were made using an Axon Multiclamp 700B amplifier (Molecular Devices) and borosilicate glass electrodes (Sutter Instrument). Signals were digitized at 10 kHz (National Instruments) and acquired using custom software written in LabVIEW (National Instruments). Data were analyzed offline using MATLAB (MathWorks). The spiking responses were recorded using the patch clamp technique in loose cell-attached mode with electrodes pulled to between three and five MU resistance and filled with Ringer's medium. In order to visualize

GCL cells in some experiments after spike recordings, neurobiotin (Vector Laboratories) and Alexa 488 (Molecular Probes) were delivered using patch pipette, pulled to between five and eight MU resistance and filled with 112.5 mM CsCH3SO3, 1 mM MgSO4, 7.8 3 10_3 mM CaCl2, 0.5 mM BAPTA, 10 mM HEPES, 4 mM ATP-Na2, 0.5 mM GTP-Na3, 5 mM lidocaine N-ethyl bromide (QX314-Br), 7.5 mM neurobiotin chloride, 13 mM Alexa 488. The pH was adjusted to 7.2 with CsOH. In pharmacological experiments, 20 mMAPB (L (+)-2-amino-4-phosphonobutyric acid, blocking metabotropic glutamate receptors) (Calbiochem) was bath-applied. Light Stimulation Photoreceptors and were stimulated with light generated by a digital light processor (DLP) projector at 75 Hz (V-339 PLUS Vision Corp.). The same DLP projector provided the infrared light for patch clamp recordings. The maximum power produced by the projector was 229 ± 35 mW/cm2 (mean ± SEM). We measured light projected through the objective lens at the focal plane on the stage. Light intensity was measured with a photodiode power meter (in Watts per cm2; Model S130VC; Thorlabs), and the spectrum was measured with a spectrometer (Model USB4000-UV-VIS; Ocean Optics). We have expressed light intensity in number of photoisomerizations per rod per second (R*/s). The light path was computer-controlled with a shutter (SC10, Thorlabs). Light intensity was modulated by neutral density filters, which were built into two filter wheels (FW102, Thorlabs).

For photoreceptor stimulation, the light was focused on the outer segments of photoreceptors in the wholemount retina. For photoreceptor stimulation the light intensity was 1.33103 R*/s. The contrast for photoreceptor stimulation was 2000. For ChR2 stimulation the light was focused on the bipolar cell layer. ChR2/H134R was activated with a 2 s light flash at _108 R*/s generated by a 120 W mercury epifluorescent lamp (X-Cite 120 PC, Lumen Dynamics). The stimulus was generated using software written in LabVIEW (National Instruments) and Python.

Conclusion

Together, the results of this thesis expand upon the current understanding of how the retina computes adaptation in identified neurons and in addition demonstrates the viability of a new set of molecular tools that will help with future studies of the nervous system.

In my work on adaptation to overall input level we found a switch like phenomenon acts in two ganglion cell types at mesopic light levels in an abrupt and reversible step-like fashion when cones become activated. In one of these cell type, PV1, we were able to dissect the circuit responsible. This switch-like phenomenon is due to the intervention of a polyaxonal wide-field amacrine cells that are connected to bipolar cells through a gap-junction. The ability to focus on genetically identifiable cell types was a de facto novelty in this project.

One open question remains whether the circuit responsible for the switch is the same for both retinal ganglion cells that show this step-like change, the PV1 and the PV6. The dissection of its input circuitry would allow us to address whether mirror ON and OFF cells would implement the same computation using the same circuitry. The fact that the same computation can be implemented by the same circuitry in two distinct pathways is still to be found and many papers have found the opposite. In this case it may be as some of the neural components are likely shared. For example, polyaxonal wide-field amacrine cell are known to exist in each layer of the inner plexiform layer (Lin & Masland 2006).
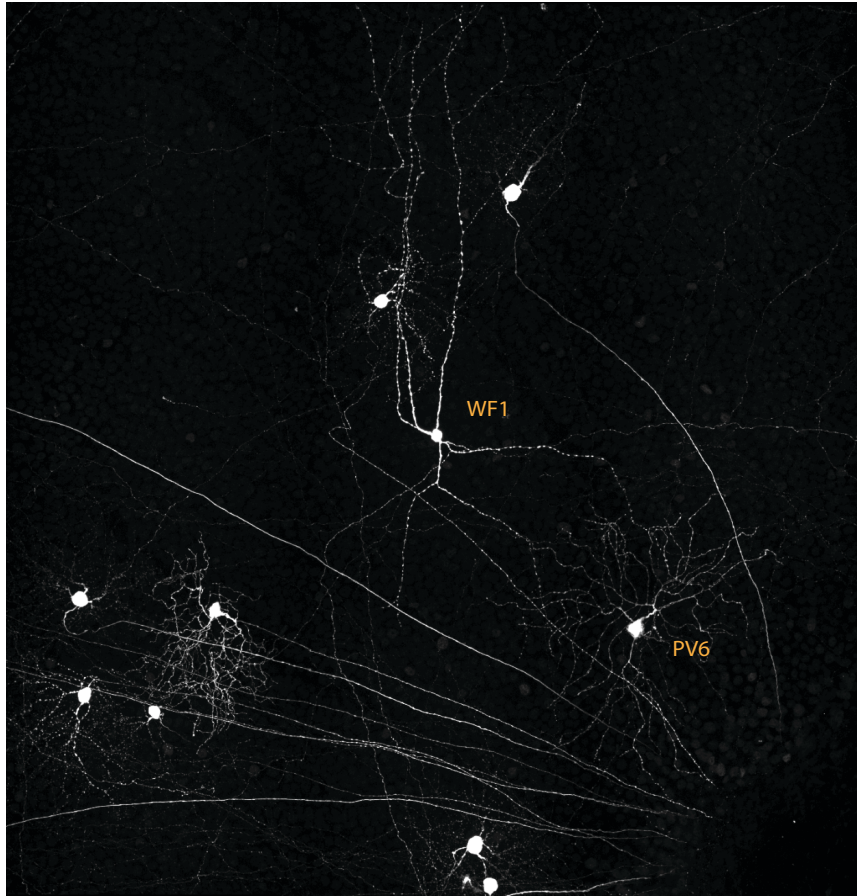
Figure 4.1. Viral tracing experiment. *Mono-transsynaptic viral tracing experiment where we can observe a single retinal ganglion cell, PV6, connected to a polyaxonal wide field amacrine cell. Reconstruction showed that the amacrine cell only connects with one ganglion cell*

The second part was focused on how the visual system adapts to contrast. We observed that at the output of the retina many cells exhibit adaptation to changes in contrast. However, we observed an ordered difference between ON and OFF cell types. We found that, for this stimulus, ON cells responded with a decrease in amplitude of the firing rate when exposed to high contrast continuously whereas OFF cells did not show the same behavior. This observation suggest that this adaptation is happening upstream of the retinal ganglion cells.

One of the possibilities that we cannot exclude was that the stimulation presented to the retina would not be the most suitable. We can see in some of the cell types that show adaptation a failure to reach a plateau, indicating that a longer stimulus may be more informative. In particular for those ganglion

cell types that exhibited very slow kinetics.

The presence of adaptation in ON cells and not in OFF cells has a number of potential explanations. The main difference between the OFF and ON pathways are located at the synapse of the cone photoreceptor and the bipolar cells responsible for the transmission of information. This difference is the type of response perpetrated by these cells to release of glutamate. ON bipolar cells have metabotropic glutamate receptors and OFF bipolar cells have ionotropic glutamate receptors so the signal transduction from the photoreceptor to bipolar cell has a range of different properties. Other possibility would be the release kinetics of glutamate from different bipolar cells, where ON bipolar cells would decrease faster the release of their neurotransmitter than the OFF bipolar cells. A third possibility would be a circuitry solution where the adaptation arises from inhibition produced from specific amacrine cells connected either to the terminal of the bipolar cell or the ganglion cell in the lower inner plexiform layer.

To try to explain why ON cells show contrast adaptation and OFF cells do not, we could use a combination of viral tracing and 2-photon calcium imaging to image the bipolar cells pre-synaptic to the parvalbumin-positive ganglion cells. Using monosynaptic restriction of a Transynaptic rabies virus we can introduce a calcium indicator in the bipolar cells connected to PV-cells. This is only possible with the help of as second virus, an Adeno-associated virus, which only infects Cre-positive cells and co-expresses TVA protein and Rabies G protein, this will restrict the infection of the Rabies virus only to AAV infected cells and help the rabies jump once since the protein necessary for this to happen is expressed by the helper virus, the rabies G protein. With the labeling of bipolar cells with a calcium indicator we can isolate the response of the bipolar cells to the contrast adaptation stimulus and with the help of pharmacology dissect the input circuit responsible for contrast adaptation in the inner retina

In the third part of my thesis I was involved in the development of a novel tool that enables us to extend the range of mouse lines where we can control genes since it uses GFP for controlling gene expression. It is potentially a very powerful tool since there are ~5000 different GFP mouse lines made for example in the Gensat project(Gong et al. 2003) that can be

used to elucidate many questions about the organization of the nervous system. Using GFP as a transcription factor we could express an optogenetic tool, channelrhodopsin in a mouse line where two types of bipolar cells are labeled with GFP. This tool was used in order to incite a response in these cells with a light stimulus, but could have been done with the expression of any other gene.

This tool gives the possibility of controlling the response of specific cell types labeled with GFP one example would be silencing parvalbumin neurons in the cortex or expressing proteins essential for the jump in transynaptic viral tracing, like the Rabies G protein This would allow us to make di-synaptic rabies jump in the retina and understand how circuits in the retina are formed since rabies would also jump from these bipolar cells to inhibitory pre-synaptic cells connected and photoreceptors.

In this thesis I have focused on how circuit mechanisms of adaptive processes are computed in the retina. From how the inner retina computes luminance from scotopic to photopic light intensity in a specific ganglion cell type to how specific ganglion cell types adapt to a change in contrast.

Bibliography

Baccus, S.A. & Meister, M., 2002. Fast and Slow Contrast Adaptation in Retinal Circuitry. *Neuron*, 36, pp.909–919.

Barlow, B.H.B., Fitzhugh, R. & Kuffler, S.W., 1957. Change of organization in the receptive fields of the cat'sretina during dark adaptation. *J. Physiol.*, pp.338–354.

Barlow, H.B., 1953. Summation and inhibition in the frog's retina. *J. Physiol.*, 119, pp.69–88.

Barlow, H.B., 1958. temporal and spacial summation in human vision at different background intensities. , pp.337–350.

Barlow, H.B. & Levick, W.R., 1969. Three factors limiting the reliable detection of light by retinal ganglion cells of the cat. *J. Physiol.*, pp.1–24.

Berry II, M.J. et al., 1999. Anticipation of moving stimuli by the retina. *Nature*, 398(March).

Berson, D.M., 2008. *Retinal ganglion cell types and their central projections. In The Senses: A Comprehensive Reference*,

Bisti, S. et al., 1977. Spatial frequency and orientation tuning curves of visual neurones in the cat: effects of mean luminance. *Exp Brain Res.*

Blakemore, C., Campbell, F.W. & Physiol, J., 1969. On the existence of neurones in the human visual system selectively sensitive to the orientation and size of retinal images.

Bloomfield, A. & Miller, F., 1986. A Functional Organization Rabbit Retina Pathways. *jounal of Neuroscience*, 6(I), pp.1–13.

Bloomfield, S.A. & Dacheux, R.F., 2001. Rod Vision: Pathways and Processing in the Mammalian Retina. *Progress in Retinal and Eye Research*, pp.1–34.

Bloomfield, S.A. & Völgyi, B., 2004. Function and plasticity of homologous coupling between AII amacrine cells. *Vision research*, 44(28), pp.3297–3306.

Caldwell, J.H., Daw, N.W. & Wyatt, H.J., 1978. Effects of picrotoxin and strychnine on rabbit retinal ganglion cells: lateral interactions for cells with more complex receptive fields. *The Journal of physiology*, 276, pp.277–298.

Caussinus, E., Kanca, O. & Affolter, M., 2012. Fluorescent fusion protein knockout mediated by anti-GFP nanobody. *Nature structural & molecular biology*, 19(1), pp.117–21.

Chalfie, M. et al., 1997. Green fluorescent protein as a marker gene expression. *Science*, 52(13 Suppl), pp.1766–7.

Chander, D. & Chichilnisky, E.J., 2001. Adaptation to temporal contrast in primate and salamander retina. *The Journal of neuroscience : the official journal of the Society for Neuroscience*, 21(24), pp.9904–16.

Chang, A.L., Wolf, J.J. & Smolke, C.D., 2012. Synthetic RNA switches as a tool for temporal and spatial control over gene expression. *Current opinion in biotechnology*, 23(5), pp.679–88.

Cook, P.B. & McReynolds, J.S., 1998. Lateral inhibition in the inner retina is important for spatial tuning of ganglion cells. *Nature neuroscience*, 1(8), pp.714–9.

Culler, S.J., Hoff, K.G. & Smolke, C.D., 2010. Reprogramming cellular behavior with RNA controllers responsive to endogenous proteins. *Science (New York, N.Y.)*, 330(6008), pp.1251–5.

Cuntz, H. et al., 2007. Robust coding of flow-field parameters by axo-axonal gap junctions between fly visual interneurons. , 104(24).

Dacheux, R.F. & Raviola, E., 1986. The rod pathway in the rabbit retina: a depolarizing bipolar and amacrine cell. *The Journal of neuroscience : the official journal of the Society for Neuroscience*, 6(2), pp.331–45.

Deans, M.R. et al., 2002. Connexin36 is essential for transmission of rod-mediated visual signals in the mammalian retina. *Neuron*, 36(4), pp.703–12.

Deans, M.R. & Paul, D.L., 2001. Mouse horizontal cells do not express connexin26 or connexin36. , 8, pp.361–366.

Dedek, K. et al., 2008. Ganglion cell adaptability: does the coupling of horizontal cells play a role? *PloS one*, 3(3), p.e1714.

Demb, J.B., 2008. Functional circuitry of visual adaptation in the retina. *The Journal of physiology*, 586(Pt 18), pp.4377–84.

DeVries, S.H. & Baylor, D. a, 1995. An alternative pathway for signal flow from rod photoreceptors to ganglion cells in mammalian retina. *Proceedings of the National Academy of Sciences of the United States of America*, 92(23), pp.10658–62.

DM, D., 1994. Physiology, morphology and spatial densities of identified ganglion cell types in primate retina. *Ciba Found Symp*, 184(12-28; discussion), pp.28–34, 63–70.

Ecker, J.L. et al., 2010. Melanopsin-Expressing Retinal Ganglion-Cell Photoreceptors: Cellular Diversity and Role in Pattern Vision. *Neuron*, 67(1), pp.49–60.

Enroth-cugell, B.Y.C. & Robson, J.G., 1966. The contrast sensitivity of retinal ganglion cells of the cat. , pp.517–552.

Enroth-cugell, C. & Lennie, P., 1975a. The control of retinal ganglion cell discharge. , pp.551–578.

Enroth-cugell, C. & Lennie, P., 1975b. The control of the retinal ganglion cell discharge. *J. Neurosci.*, pp.551–578.

Estevez, M.E. et al., 2012. Form and function of the M4 cell, an intrinsically photosensitive retinal ganglion cell type contributing to geniculocortical vision. *The Journal of neuroscience : the official journal of the Society for Neuroscience*, 32(39), pp.13608–20.

Fain, G.L. et al., 2001. Adaptation in vertebrate photoreceptors. *Physiological reviews*, 81(1), pp.117–151.

Farrow, K. & Masland, R.H., 2011. Physiological clustering of visual channels in the mouse retina. , pp.1516–1530.

Feng, G. et al., 2000. Imaging neuronal subsets in transgenic mice expressing multiple spectral variants of GFP. *Neuron*, 28(1), pp.41–51.

Field, G.D., Sampath, A.P. & Rieke, F., 2005. Retinal processing near absolute threshold: from behavior to mechanism. *Annual review of physiology*, 67, pp.491–514.

Flores-Herr, N., Protti, D. a & Wässle, H., 2001. Synaptic currents generating the inhibitory surround of ganglion cells in the mammalian retina. *The Journal of neuroscience : the official journal of the Society for Neuroscience*, 21(13), pp.4852–63.

Fried, S.I., Munch, T.A. & Werblin, F.S., 2002. Mechanisms and circuitry underlying directional selectivity in the retina. *Nature*, 420, pp.411–414.

Geisler, W.S., 2008. Visual perception and the statistical properties of natural scenes. *Annual review of psychology*, 59, pp.167–92.

Ghosh, K.K. et al., 2004. Types of bipolar cells in the mouse retina. *The Journal of Comparative Neurology*, 469(1), pp.70–82.

Gong, S. et al., 2003. A gene expression atlas of the central nervous system based on bacterial artificial chromosomes. *Nature*, 425(6961), pp.917–25.

Green, D. & Powers, M., 1982. Mechanisms of light adaptation in rat retina. *Vision research*, pp.209–216.

Hippenmeyer, S. et al., 2005. A developmental switch in the response of DRG neurons to ETS transcription factor signaling. *PLoS biology*, 3(5), p.e159.

Hood, D.C. & Finkelstein, M., 1986. *Sensitivity to light. In Handbook of Perception and Human Performance*,

Hu, E.H. et al., 2010. Light increases the gap junctional coupling of retinal ganglion cells. *The Journal of physiology*, 588(Pt 21), pp.4145–63.

Huang, L. et al., 2003. G protein subunit G gamma 13 is coexpressed with G alpha o, G beta 3, and G beta 4 in retinal ON bipolar cells. *The Journal of comparative neurology*, 455(1), pp.1–10.

Huberman, A.D. et al., 2008. Architecture and activity-mediated refinement of axonal projections from a mosaic of genetically identified retinal ganglion cells. *Neuron*, 59(3), pp.425–38.

Huberman, A.D. et al., 2009. Genetic identification of an On-Off direction-selective retinal ganglion cell subtype reveals a layer-specific subcortical map of posterior motion. *Neuron*, 62(3), pp.327–34.

Ichinose, T. & Lukasiewicz, P.D., 2007. Ambient light regulates sodium channel activity to dynamically control retinal signaling. *The Journal of neuroscience : the official journal of the Society for Neuroscience*, 27(17), pp.4756–64.

Ichinose, T. & Lukasiewicz, P.D., 2005. Inner and outer retinal pathways both contribute to surround inhibition of salamander ganglion cells. *The Journal of physiology*, 565(Pt 2), pp.517–35.

Jobling, S. a et al., 2003. Immunomodulation of enzyme function in plants by single-domain antibody fragments. *Nature biotechnology*, 21(1), pp.77–80.

Kay, J.N. et al., 2011. Retinal ganglion cells with distinct directional preferences differ in molecular identity, structure, and central projections. *The Journal of neuroscience : the official journal of the Society for Neuroscience*, 31(21), pp.7753–62.

Kelly, D., 1972. adaptation effects on spatio-temporal sine-wave thresholds. *Vision research*, pp.89–101.

Kim, I.-J. et al., 2008. Molecular identification of a retinal cell type that responds to upward motion. *Nature*, 452(7186), pp.478–82.

Kirchhofer, A. et al., 2010. Modulation of protein properties in living cells using nanobodies. *Nature structural & molecular biology*, 17(1), pp.133–8.

Kong, J. et al., 2005. Diversity of ganglion cells in the mouse retina: Unsupervised morphological classification and its limits. *The Journal of Comparative Neurology*, 489(3), pp.293–310. Available at: papers://d675cf12-f2bd-4bee-8039-a57b4bfd73dc/Paper/p65.

Kuffler, S.W., 1953. Discharge patterns and functional mammalian retina. *J Neurophysiol.*, 16(1), pp.37–68.

Kurahashi, T. & Menini, A., 1997. Mechanism of odorant adaptation in the olfatory receptor cell. *Nature*, 385, pp.725, 726, 727, 728, 729.

Lanting, C.P. et al., 2013. Mechanisms of adaptation in human auditory cortex. *Journal of neurophysiology*, 110(4), pp.973–83. Available at: http://www.ncbi.nlm.nih.gov/pubmed/23719212 [Accessed February 3, 2014].

Lasater, E.M., 1987. Retinal horizontal cell gap junctional conductance is modulated by dopamine through a cyclic AMP-dependent protein kinase.

Proceedings of the National Academy of Sciences of the United States of America, 84(20), pp.7319–23.

Levick, W.R., 1967. Receptive fields and trigger features of ganglion cells in the visual streak of the rabbits retina. *The Journal of physiology*, 188(3), pp.285–307. Available at: http://jp.physoc.org/content/188/3/285.long.

Lin, B. & Masland, R.H., 2006. Populations of wide-field amacrine cells in the mouse retina. *The Journal of Comparative Neurology*, 499(5), pp.797–809.

Lyubarsky, A.L. et al., 1999. UV- and Midwave-Sensitive Cone-Driven Retinal Responses of the Mouse : A Possible Phenotype for Coexpression of. , 19(1), pp.442–455.

MacNeil, M. a et al., 2004. The population of bipolar cells in the rabbit retina. *The Journal of comparative neurology*, 472(1), pp.73–86.

Madisen, L. et al., 2010. A robust and high-throughput Cre reporting and characterization system for the whole mouse brain. *Nature neuroscience*, 13(1), pp.133–40.

Mangel, B.Y.S.C., 1991. Analysis of the horizontal cell contribution to the receptive field surround og ganglion cells in the rabbit retina. , (1991), pp.211–234.

Mangel, S.C. & Dowling, J.E., 1985. Responsiveness and receptive field size of carp horizontal cells are reduced by prolonged darkness and dopamine. *Science (New York, N.Y.)*, 229(4718), pp.1107–9.

Manookin, M.B. et al., 2008. Disinhibition Combines with Excitation to Extend the Operating Range of the OFF Visual Pathway in Daylight. , 28(16), pp.4136–4150.

Manookin, M.B. & Demb, J.B., 2006. Presynaptic mechanism for slow contrast adaptation in mammalian retinal ganglion cells. *Neuron*, 50(3), pp.453–64.

Mante, V. et al., 2005. Independence of luminance and contrast in natural scenes and in the early visual system. *Nature neuroscience*, 8(12), pp.1690–7.

Marshel, J.H. et al., 2010. Targeting Single Neuronal Networks for Gene Expression and Cell Labeling In Vivo. *Neuron*, 67(4), pp.562–574.

Masland, R.H., 2001a. Neuronal diversity in the retina. *Current opinion in neurobiology*, 11(4), pp.431–6.

Masland, R.H., 2001b. The fundamental plan of the retina. *Nature neuroscience*, pp.1–10.

McMahon, M.J., Packer, O.S. & Dacey, D.M., 2004. The classical receptive field surround of primate parasol ganglion cells is mediated primarily by a non-GABAergic pathway. *The Journal of neuroscience : the official journal of the Society for Neuroscience*, 24(15), pp.3736–45.

Mills, S. & Massey, S., 1995. differential properteis of two gap junctional pathways made by AII amacrine cells.

Muller JF, D.R., 1997. Alpha ganglion cells of the rabbit retina lose antagonistic surround responses under dark adaptation. *Vis Neurosci.*, pp.395–401.

Münch, T.A. et al., 2009. Approach sensitivity in the retina processed by a multifunctional neural circuit. *Nature neuroscience*, 12(10), pp.1308–1316.

Nagel, G. et al., 2005. Light activation of channelrhodopsin-2 in excitable cells of Caenorhabditis elegans triggers rapid behavioral responses. *Current biology : CB*, 15(24), pp.2279–84.

Naka, B.K. & Witkovsky, P., 1972. Dogfish ganglion cell discharge resulting from extrinsic polarization of the horizontal cells. *J. Physiol.*, 223, pp.449–460.

Nathan, J. et al., 2006. Scotopic and photopic visual thresholds and spatial and temporal discrimination evaluated by behavior of mice in a water maze. *Photochemistry and photobiology*, 82(6), pp.1489–94.

Van Nes, F. et al., 1967. Spatiotemporal modulation transfer in the human eye. *J Opt Soc Am.*

Nikonov, S.S. et al., 2005. Photoreceptors of Nrl ϒ / ϒ Mice Coexpress Functional S- and M-cone Opsins Having Distinct Inactivation Mechanisms. , 125(March).

Nikonov, S.S. et al., 2006. Physiological Features of the S- and M-cone Photoreceptors of Wild-type Mice from Single-cell Recordings. , 127(4), pp.359–374.

Pang, J.-J., Gao, F. & Wu, S.M., 2003. Light-evoked excitatory and inhibitory synaptic inputs to ON and OFF alpha ganglion cells in the mouse retina. *The Journal of neuroscience : the official journal of the Society for Neuroscience*, 23(14), pp.6063–73.

Pasternak, T. & Merigann, W.H., 1981. The luminance dependence of spatial vision in the cat. *Vision research*.

Peichl, L. & Wässle, H., 1983. The structural correlate of the receptive field centre of alpha ganglion cells in the cat retina. *The Journal of physiology*, 341(1983), pp.309–24.

Pennesi, M.E., Lyubarsky, a L. & Pugh, E.N., 1998. Extreme responsiveness of the pupil of the dark-adapted mouse to steady retinal illumination. *Investigative ophthalmology & visual science*, 39(11), pp.2148–56.

Protti, D.A. et al., 2005. Light Signaling in Scotopic Conditions in the Rabbit , Mouse and Rat Retina : A Physiological and Anatomical Study. , pp.3479–3488.

Pugh, E.J. & Lamb, T., 1993. Amplification and kinetics of the activation steps in phototransduction. *Biochim Biophys Acta.*

Ramoa, a S., Freeman, R.D. & Macy, A., 1985. Comparison of response properties of cells in the cat's visual cortex at high and low luminance levels. *Journal of neurophysiology*, 54(1), pp.61–72.

Ribelayga, C., Cao, Y. & Mangel, S.C., 2008. The circadian clock in the retina controls rod-cone coupling. *Neuron*, 59(5), pp.790–801.

Rieke, F. & Rudd, M.E., 2009. The challenges natural images pose for visual adaptation. *Neuron*, 64(5), pp.605–16.

Rodieck, R. & Stone, J., 1965. Analysis of receptive fields of cat retinal ganglion cells. *Journal of neurophysiology*.

Roska, B., Nemeth, E. & Werblin, F.S., 1998. Response to Change Is Facilitated by a Three Neuron Disinhibitor y Pathway in the Tiger Salamander Retina. *The Journal of Neuroscience*, pp.1–9.

Roska, B. & Werblin, F., 2001. Vertical interactions across ten parallel, stacked representations in the mammalian retina. *Nature*, 410(6828), pp.583–587.

Sena-Esteves, M. et al., 2004. Optimized large-scale production of high titer lentivirus vector pseudotypes. *J. Virol. Methods*, 122, pp.131–139.

Seung, H.S. & Sompolinsky, H., 1993. Simple models for reading neuronal population codes. *Proceedings of the National Academy of Sciences of the United States of America*, 90(22), pp.10749–53.

Shapley, R.M. & Enroth-Cugell, C., 1984. *Visual adaptation and retinal gain controls. Prog. Retinal Res*,

Siegert, S. et al., 2009. Genetic address book for retinal cell types. *Nature neuroscience*, 12(9), pp.1197–1204.

Siegert, S. et al., 2012. Transcriptional code and disease map for adult retinal cell types. *Nature neuroscience*, 15(3), pp.487–495.

Smirnakis, S. et al., 1997. Adaptation of retinal processing to image contrast and spatial scale. *Nature*, 386(6620), pp.69–73.

Stepien, A.E., Tripodi, M. & Arber, S., 2010. Monosynaptic Rabies Virus Reveals Premotor Network Organization and Synaptic Specificity of Cholinergic Partition Cells. *Neuron*, 68(3), pp.456–472.

Troy, J.B., Bohnsack, D.L. & Diller, L.C., 1999. Spatial properties of the cat X-cell receptive field as a function of mean light level. *Visual Neuroscience*.

Truchard, a M., Ohzawa, I. & Freeman, R.D., 2000. Contrast gain control in the visual cortex: monocular versus binocular mechanisms. *The Journal of neuroscience : the official journal of the Society for Neuroscience*, 20(8), pp.3017–32.

Tsien, R.Y., 1998. The green flouresncent. *annual review of biochemestry*, 67, pp.509–44.

Umino, Y., Solessio, E. & Barlow, R.B., 2008. Speed, spatial, and temporal tuning of rod and cone vision in mouse. *The Journal of neuroscience : the official journal of the Society for Neuroscience*, 28(1), pp.189–98.

De Valois, R., Morgan, H. & Snodderly, D., 1974. Psychophysical studies of monkey vision. 3. Spatial luminance contrast sensitivity tests of macaque and human observers.

Victor Jonathan D., 1987. The dynamics of the cat retinal x cell centre. *J. Physiol. (Lond.)*, pp.219–246.

Virsu, V., Lee, B. & Creutzfeldt, O., 1977. Dark adaptation and receptive field organisation of cells in the cat lateral geniculate nucleus. *Exp Brain Res.*

De Vries, B.Y.S.H. & Schwartz, E.A., 1989. Modulation of an electrical synapse between solitary pairs of catfish horizontal cells by dopamine and second messengers. , (1989), pp.351–375.

Wässle, H. et al., 2009. Glycinergic transmission in the Mammalian retina. *Frontiers in molecular neuroscience*, 2, p.6.

Wässle, H., 2004. Parallel processing in the mammalian retina. *Nature Reviews Neuroscience*, 5(10), pp.1–11.

Watson, A., Barlow, H. & Robson, J., 1983. What does the eye see best? *Nature*, 302(5907), pp.419–22.

Werblin, F.S., 1974. Control of Retinal Sensitivity: II. Lateral Interactions at the Outer Plexiform Layer. *The Journal of General Physiology*, 63(1), pp.62–87.

Wickersham, I.R., Sullivan, H.A. & Seung, H.S., 2010. Production of glycoprotein-deleted rabies viruses for monosynaptic tracing and high-level gene expression in neurons. *Nature protocols*, 5(3), pp.595–606.

Wiesel, T.N. & Hubel, D.H., 1966. Spatial and chromatic interections the lateral body of the rhesus. *J Neurophysiol.*, 29(6), pp.1115–56.

Witkovsky, P., 2004. Dopamine and retinal function. *Doc Ophthalmol.*, 108(1), pp.17–40.

WR., T., 1999. TTX attenuates surround inhibition in rabbit retinal ganglion cells. *Vis Neurosci.*

Wurch, T., Pierré, A. & Depil, S., 2012. Novel protein scaffolds as emerging therapeutic proteins: from discovery to clinical proof-of-concept. *Trends in biotechnology*, 30(11), pp.575–82.

Xin, D. & Bloomfield, S. a, 1999. Dark- and light-induced changes in coupling between horizontal cells in mammalian retina. *The Journal of comparative neurology*, 405(1), pp.75–87.

Yang, J. & Stevenson, S.B., 1999. Post-retinal processing of background luminance. *Vision research*, 39(24), pp.4045–51.

Yizhar, O. et al., 2011. Optogenetics in neural systems. *Neuron*, 71(1), pp.9–34.

Yonehara, K. et al., 2011. Spatially asymmetric reorganization of inhibition establishes a motion-sensitive circuit. *Nature*, 469(7330), pp.407–410.

Zaghloul, K. a et al., 2007. Functional circuitry for peripheral suppression in Mammalian Y-type retinal ganglion cells. *Journal of neurophysiology*, 97(6), pp.4327–40.

Zhang, J., Jung, C. & Slaughter, M., 1997. Serial inhibitory synapses in retina. *Visual Neuroscience*.

Zhang, Y. et al., 2012. The most numerous ganglion cell type of the mouse retina is a selective feature detector. *Proceedings of the National Academy of Sciences of the United States of America*, 109(36), pp.E2391–8.

Acknowledgments

First I would like to thank my thesis committee, Dr. Botond Roska, Prof. Dr. Silvia Arber and Prof. Dr. Klaus Conzelmann for their time given to my thesis and their excellent support in my thesis committee meetings.

I would like to thank Botond especially since he gave the opportunity to continue my studies in an amazing group, I have learned a great deal from him, not only about science but also about life.

I would like to thank all the members of the Roska group, past and present for valuable discussions and help in many situations. I would like to give a special thanks to Dr. Karl Farrow, whose valuable contribution and orientation was indispensable for my studies, and to Dr. Tamas Szikra for valuable discussions. To Dr. Keizuke Yonehara for all the teaching in variety of different techniques and Dr. Kamill Balint for the help with the virology. To Brigitte Gross Scherf that without her the laboratory would not function and Sabrina Djaffer for providing me all the mice needed. I will also like to thank the FMI microscope facility for all the help in acquiring and analyzing my data. Finally I would like to thank my family, especially my mother for all the life advices and support, and Lara for all the support given.

Curriculum Vitae

PERSONAL DATA

Name	**Miguel** Henriques dos Santos Caracol **Teixeira**
Adress	Davidsbodenstrasse 5, 4056 Basel, Switzerland
Contacts	Mobile +41 78 737 12 85
E-mail	miguelcteixeira@gmail.com
Date of Birth	11 of March 1980
Nationality	Portuguese
Marital status	Single
Swiss Permit	C until 31.10.2018
Availability	July 2014

EDUCATION AND TRAINING

2014	PhD in Neurosciences, "Luminance and contrast adaptation of the inner retina" University of Basel, April 2014
2009 – 2014	PhD candidate University of Basel, supervised by Botond Roska, *Friedrich Miescher Institute*, Basel Switzerland
2008 – 2009	PhD student, Frontiers in Genetics' PhD program, NCCR- Rotation at laboratory, EPFL Prof. Joachim Lingner Rotation at laboratory, Universite de Geneve Prof. David Shore
2002 – 2008	Diploma in Biology in *Universidade Lusófona de Humanidade e Tecnologias* (5 years studies) with an average of 15

ACADEMIC WORK

April 2014 – to date	Post-doc at Structure and Function of Neural Circuits laboratory of Botond Roska at Friedrich Miescher Institute, Basel Switzerland
2009 – 2014	PhD candidate at Friedrich Miescher Institute, Basel, Switzerland, with the supervision of Botond Roska in Retina Neuroscience
2008 – 2009 classes and rotations	Member of the 2008 PhD programme "NCCR-Frontiers-in-genetics"
2007 – 2008	Diploma thesis at the Instituto Gulbenkian de Ciência in the group of Telomere and Genome Stability, with the supervision of Miguel Godinho Ferreira (diploma student), involved in three different projects: "What is the fate of a chromosome fusion"; "Will a double-

strand break in a telomere be recognized by the cell"; "A new technology in fission yeast to turn genes on and off"

2004 – 2006 Undergraduate research training at the Instituto Gulbenkian de Ciência's Malária Mitogens Laboratory. With the supervision of Professor António Coutinho on the project "The role of cyclophiline in malaria"

Courses

LTK-1 animal course – necessary for animal work in Europe
Mathematica – functional programming course

PUBLICATIONS

*Farrow K, **Teixeira M**, Szikra T, Viney TJ, Balint K, Yonehara K, Roska B* Ambient illumination toggles a neuronal circuit switch in the retina and visual perception at cone threshold. Neuron 78: 325-338 (2013)

*Yonehara K, Farrow K, Ghanem A, Hillier D, Balint K, **Teixeira M**, Jüttner J, Noda M, Neve RL, Conzelmann KK, Roska B* The first stage of cardinal direction selectivity is localized to the dendrites of retinal ganglion cells Neuron 79:1078-1085 (2013)

Tang, J.D., Szikra, T., Kozorovitskiy, Y., **Teixeira, M**. Sabatini, B.L., Roska, B. and Cepko, C.L. 2013. *Cell* 154:928–939

PRESENTATIONS AND POSTERS (selected)

Teixeira, M., Farrow, K., Balint, K., Yonehara, K., Roska, B. "The mechanism of contrast adaptation in the retina". FMI annual Meeting, 2013, Arosa, Switzerland

Teixeira, M., Farrow, K., Balint, K., Yonehara, K., Roska, B. "Ambient illumination toggles a neuronal circuit switch in the retina and visual perception at cone threshold". NCCR Frontiers-in-genetics. 2013, Saas Fee, Switzerland

Teixeira, M., Balint, K., Yonehara, K., Farrow, K., Roska, B. "The retinal circuitry in scotopic and photopic conditions"; European Retina Meeting. 2011, Amsterdam, The Netherlands

Teixeira, M., Godinho-Ferreira, M. "A new technology in fission yeast to turn genes on and off"; EMBO Telomere meeting. 2008 Villars-sur-Ollon, Switzerland

METHODS AND SKILLS

Molecular biology: cell culture, cloning, immunohistochemistry, PCR, Western blot, southern blot, and Northern blot

Electrophysiology: Optogenetics, Single-cell Patch clamp recordings, single loose-cell patch-clamp recording, analysis on Matlab, retina whole-mount preparations, retinal slices preparations.

Microscopy: Two-photon imaging, calcium-imaging, confocal imaging

Virology: production of Rabies virus, production of Adeno-associated virus

SPORTS CARREER

Member of the Novartis Sports club Football Team 2012- to date
Rugby player of Sport Lisboa e Benfica (1993- 2008), Captain of the senior squad 2007-2008
Member of Portuguese National Rugby team youth and senior (1996-2006)

LANGUAGE

Portuguese (mother tongue); English (proficiency); French (average)

STUDENT ACTIVITIES

2005 to 2007 – President of the student counsel of students of biology

FELLOWSHIPS

Swiss National Science Foundation National Centre of Competence in research – Frontiers in Genetics PhD Fellowship